Environmental Controls on Observed Spatial Variability of Soil Pore Water Geochemistry in Small Headwater Catchments Underlain with Permafrost

Nathan Alec Conroy,[1][*] Jeffrey M. Heikoop,[1] Emma Lathrop,[1,2] Dea Musa,[1] Brent D. Newman,[1] Chonggang Xu,[1] Rachael E. McCaully,[3] Carli A. Arendt,[3] Verity G. Salmon,[4] Amy Breen,[5] Vladimir Romanovsky,[6] Katrina E. Bennett,[1] Cathy J. Wilson,[1] and Stan D. Wullschleger[4]

[1]Earth and Environmental Sciences Division, Los Alamos National Laboratory, Bikini Atoll Road, Los Alamos, New Mexico, 87545, USA
[2]Center for Ecosystem Science and Society, Department of Biological Sciences, Northern Arizona University, Flagstaff, AZ, 86011, USA
[3]Department of Marine Earth and Atmospheric Sciences, North Carolina State University, Raleigh, North Carolina, 27695, USA
[4]Biological and Environmental Systems Science Division and Climate Change Science Institute, Oak Ridge National Laboratory, Oak Ridge, Tennessee, 37831, USA
[5]International Arctic Research Center, P.O. Box 757340, University of Alaska, Fairbanks, Alaska 99775-7340, USA
[6]Geophysical Institute, University of Alaska Fairbanks, Fairbanks, Alaska, 99775, USA

Correspondence to: Nathan Alec Conroy (nconroy@lanl.gov)

Abstract. Soil pore water (SPW) chemistry can vary substantially across multiple scales in Arctic permafrost landscapes. The magnitude of these variations and their relationship to scale are critical considerations for understanding current controls on geochemical cycling and for predicting future changes. These aspects are especially important for Arctic change modelling where accurate representation of sub-grid variability may be necessary to predict watershed scale behaviours. Our research goal was to characterize intra- and inter-watershed soil water geochemical variations at two contrasting locations in the Seward Peninsula of Alaska, USA. We then attempt to establish which environmental factors were important for controlling concentrations of important pore water solutes in these systems. The SPW geochemistry of 18 locations spanning two small Arctic catchments were examined for spatial variability and its dominant environmental controls. The primary environmental controls considered were vegetation, soil moisture/redox condition, water/soil interactions and hydrologic transport, and mineral solubility. The sampling locations varied in terms of vegetation type and canopy height, presence or absence of near-surface permafrost, soil moisture, and hillslope position. Vegetation was found to have a significant impact on SPW NO_3^- concentrations, associated with the localized presence of nitrogen-fixing alders and mineralization and nitrification of leaf litter from tall willow shrubs. The elevated NO_3^- concentrations were however, frequently equipoised by increased microbial denitrification in regions with sufficient moisture to support it. Vegetation also had an observable impact on soil moisture sensitive constituents, but the effect was less significant. The redox conditions in both catchments were generally limited by Fe reduction, seemingly well-buffered by a cache of amorphous Fe hydroxides, with the most reducing conditions found at sampling locations with the highest soil moisture content. Non-redox-sensitive cations were affected by a wide variety of water-soil interactions that affect mineral solubility and transport. Identification of the dominant controls on current SPW hydrogeochemistry allows for qualitative prediction of future geochemical trends in small Arctic catchments that are likely to experience warming and permafrost thaw. As source

39 areas for geochemical fluxes to the broader Arctic hydrologic system, geochemical processes occurring in these
40 environments are particularly important to understand and predict with regards to such environmental changes.

41 **1. Introduction**

42 Permafrost thaw in the Arctic is causing significant changes to landscape structure (Kokelj and Jorgenson, 2013;
43 Rowland et al., 2010), hydrology (Hiyama et al., 2021; Kurylyk et al., 2021; Liljedahl et al., 2016; Vonk, Tank, and
44 Walvoord, 2019; Walvoord and Kurylyk, 2016), vegetation (Lara et al., 2018; Myers-Smith et al., 2011; Sturm,
45 Racine, and Tape, 2001; K. D. Tape et al., 2012; Tape, Sturm, and Racine, 2006;), and biogeochemistry (O'Donnell
46 et al., 2021; Frey and McClelland, 2009; Salmon et al., 2019; Vonk, Tank, and Walvoord, 2019). The integrated
47 hydrogeochemical effects of these environmental changes are already apparent in the chemistry of the large Arctic
48 rivers, where fluxes of carbon and nutrients are increasing, leading to enhanced nutrient loadings, with strong
49 implications for the global carbon cycle (Bring et al., 2016; Fuchs et al., 2020; McClelland et al., 2016). While the
50 watershed areas of large Arctic rivers are vast, recent studies suggest that solute concentrations in these large rivers
51 are likely controlled by solute generation processes occurring at much smaller scales (Harms and Ludwig, 2016; Koch
52 et al., 2013; Shogren et al., 2019; Vonk et al., 2015).
53 While there is a rapidly growing body of literature focused on observing and understanding environmental changes
54 over time with further Arctic warming, relatively few studies directly address the existing spatial variability, within
55 catchments or across catchments, and we are not aware of any studies that have combined field observations with
56 thermodynamic modelling in an effort to understand the causes of the existing spatial variability. Therefore, we have
57 a limited understanding of the key environmental controls on the spatial distribution of soil pore water solute
58 concentrations. In this study, we quantitatively evaluate the spatial variability of soil pore water (SPW) geochemistry
59 within and between two distinct catchments underlain with permafrost, and then seek to identify the source of the
60 observed spatial variability.
61 This study takes advantage of a scientifically diverse array of observations and datasets made available by the Next
62 Generation Ecosystem Experiment (NGEE) Arctic project, sponsored by the US Department of Energy Office of
63 Science. Most of the locations studied herein were selected by the NGEE Arctic project to provide co-located
64 measurements in a wide range of vegetation types, nested within representative hillslopes and catchments. Although
65 selected largely to represent a range of vegetation structure, such as shrub abundance and canopy height, these
66 locations also have considerable variability in other environmental parameters including, but not limited to: soil
67 moisture and temperature, presence or absence of near-surface permafrost, and maximum observed thaw depth (**Table
68 1** and **Table 2**). The vegetation-delineated sampling approach provides an opportunity to not only quantify the
69 biogeochemical variability of SPW in Arctic environments, but also to investigate the root causes of that observed
70 variability. Data from additional sampling locations, available from a co-located study, were also utilized when
71 possible.
72 Our overarching hypothesis is that vegetation-type and hillslope position are the dominant controls on spatial
73 variability of SPW geochemistry at the NGEE Arctic field sites located on the Seward Peninsula. Vegetation-type
74 seems likely to have a significant effect on SPW geochemistry both directly and indirectly. Indirect effects would

75   include vegetation canopy impacts on soil moisture (through evapotranspiration and snow trapping). Direct effects of

76   vegetation would include nutrient cycle changes resulting from the annual deposition of plant litter. Such a direct

77   effect can be augmented at sites populated by alder shrubs due to this genus of deciduous shrubs ability to form a

78   symbiotic relationship with nitrogen-fixing *Frankia,* which they host in underground root nodules. Nitrogen fixation

79   associated with alders has previously been shown to accelerate local nitrogen cycling (Binkley et al., 1992; Clein and

80   Schimel, 1995; Bühlmann et al., 2014). Soil moisture will also affect SPW geochemistry, particularly of redox

81   sensitive species, by limiting oxygen diffusion and thus controlling which regions develop anoxic/reducing

82   geochemical conditions. Soil moisture impacts will likely be correlated with vegetation-type as well as hillslope

83   position, and the presence or absence of perching layers, including permafrost, all of which impact the vertical and

84   horizontal drainage characteristics of a watershed. Chemical species that are not redox-sensitive or controlled by

85   biogeochemical reactions are likely to be affected by transport, solubility, and water/sediment/organic matter

86   interactions, and therefore largely controlled by hillslope position as well as soil moisture.

87   Identifying the dominant controls on solute concentration variability within each catchment and across catchments

88   will facilitate better projections of future soil pore hydrogeochemistry in permafrost landscapes, and how these

89   signatures are related to changing soil moisture and increasing tundra shrub abundance in a changing Arctic (Bring et

90   al., 2016; Myers-Smith et al., 2011; Prowse et al., 2015; Salmon et al., 2019; Sturm et al., 2001; Tape et al., 2012;

91   Tape et al., 2006; Wrona et al., 2016, 2016). Arctic warming and associated permafrost thaw will increase hydrological

92   connectedness between terrestrial and aquatic environments through deepening of the active layer and the formation

93   of deeper, more coherent groundwater flow paths (Bring et al., 2016; Harms and Jones, 2012; Prowse et al., 2015a;

94   Prowse et al., 2015b). Meanwhile, changes in hydrogeochemical signatures in larger Arctic rivers are likely to

95   originate in smaller catchments (McClelland et al., 2016; Prowse et al., 2015; Shogren et al., 2019; Spence et al.,

96   2015). In this sense, changes in hydrogeochemistry in small Arctic catchments not only impact hydrogeochemistry at

97   much larger scales, but also prognosticate the future hydrogeochemistry of larger Arctic rivers.

2. Methods

2.1 Site Descriptions

100   This study focuses on two sites with permafrost on the Seward Peninsula of western Alaska, the Teller-27 Catchment

101   and the Kougarok-64 Hillslope (**Figure 1**). The Teller-27 Catchment, henceforth "Teller," is a small (~2.25 km^2)

102   headwater catchment located west of mile marker 27 along the Nome-Teller Highway northwest of Nome, Alaska.

103   The Kougarok-64 Hillslope, henceforth "Kougarok," is a hillslope (~2.0 km^2) located west of mile marker 64 along

104   the Nome-Taylor Highway northeast of Nome, Alaska. We utilized data from "intensive stations" at both Teller and

105   Kougarok where concentrated, multi-year, co-located observations of soil water chemistry, vegetation characteristics,

106   soil moisture and temperature, and other measurements have been collected as part of the NGEE Arctic Research

107   Project. These are identified as TL# (Teller Station #) or KG# (Kougarok Station #) in **Figure 2** and **Figure 3**,

108   respectively. It should be noted that Teller and Kougarok are not "paired watersheds" in the classical sense, differing

109   in only one major characteristic, which provides the basis for comparison. Instead, Teller and Kougarok differ in many

110   respects and are both representative of the broad range of hillslope conditions common on the Seward Peninsula.

111   Detailed descriptions of Teller and Kougarok have been published previously (Jafarov et al., 2018; Léger et al., 2019;

112   Philben et al., 2019, 2020; Salmon et al., 2019; Yang et al., 2020), therefore, only the catchment characteristics that

113   are probable sources of variability in SPW chemistry will be highlighted here.

114   Teller is a discrete catchment with a well-defined central drainage, a vertical declivity of approximately 200 m, and a

115   catchment area of approximately 2.25 km^2. Temperature probes, soil pits, coring activities, and geophysical

116   interpretations at Teller have confirmed the catchment is underlain with discontinuous permafrost (Léger et al., 2019).

117   The upper shoulder of Teller (near Station 5, **Figure 2** and **Figure 5**) is underlain with near-surface permafrost and

118   appears to be a degraded peat plateau. The resultant microtopography of the degraded peat and the shallow perching

119   horizon caused by the permafrost creates a landscape of unsaturated peat mounds surrounded by ponds and saturated

120   soils. Downslope of the peat plateau, the Teller hillslope has highly variable soil moisture and vegetation (**Table 1**).

121   The microtopography within the lower footslope looks similar to the upper shoulder, but the peat appears more

122   severely degraded and the cause of the perched water table is less clear. Léger et al. (2019) suggest the presence of

123   permafrost at a depth of 1 – 2 m at Teller Station 9 (**Figure 2**), but the perching could also be caused by a layer of silt,

124   at a depth of approximately 30 cm (Graham et al., 2018). The full extent of permafrost and silt in this region of the

125   catchment remains unknown, but the thaw depth in July 2018 was greater than 1 m and maintained a perched water

126   table (Philben et al., 2020), suggesting perching could be the result of silt rather than permafrost. Vegetation type,

127   moisture content, permafrost extent, and hillslope position for all Teller Stations are summarized in **Table 1**.

128   Kougarok differs in many ways from Teller, although both have characteristics that are typical of hillslopes on the

129   Seward Peninsula. Kougarok is a convex hillslope, with a vertical declivity of approximately 70 meters. The study

130   area at Kougarok is approximately 2.0 km^2. Soil temperature measurements at Kougarok suggest that the vast majority

131   of the site is underlain by shallow continuous permafrost (Romanovsky, Cable, and Dolgikh, 2020a); Kougarok

132   Station 5 is an exception, where the permafrost is deeper (Romanovsky et al., 2020a). The upper shoulder of Kougarok

133   is a well-drained rocky outcrop composed of metagranitic rock (Hopkins et al., 1955; Till, Dumoulin, Werdon, and

134   Bleick, 2011). Saturated soils are not prevalent until the footslope and the lower backslope, where Kougarok Stations

135   2, 11, 10, 1, and 6 are situated (**Figure 3**). The lower backslope is characterized by persistent saturation between

136   ubiquitous tussocks, formed by the tussock cotton grass Eriophorum vaginatum. The tussock-lichen tundra at

137   Kougarok introduces microtopography and spatially variable saturation; in this sense, the Kougarok tussocks are

138   analogous to the peat mounds and hummocks at Teller, but on different spatial scales and formed by different

139   processes. Kougarok has numerous patches of alder shrubland in an altitudinal band within the upper backslope; it

140   should be emphasized that Teller lacks tussock-lichen tundra and alder (Alnus viridis ssp. fruticosa) shrubs that are a

141   feature of Kougarok. While continuous permafrost largely remains, the Kougarok site appears to be undergoing

142   environmental changes as evidenced by an increase in alder coverage over the past decades (Salmon et al., 2019). Soil

143   profiles underneath the alder patches are rocky with shallow bedrock and warmer permafrost (**Table 2**). Shrub tundra

144   (alder savanna in tussock tundra and willow-birch tundra) dominates the lower backslope, where the annual active

145   layer thickness is typically less than 100 cm. Vegetation type, moisture content, permafrost extent, and hillslope

146   position at all Kougarok stations are summarized in **Table 2**.

2.2 Sampling & Analytical Approach

SPWs were sampled using two complimentary techniques. Fiberglass wicks (Frisbee et al., 2010) were deployed in the upper 30 cm of soils at stations where shallow soils were unsaturated. These wicks were left in place from year-to-year and only replaced if damage was observed or suspected. The sample reservoirs from the wicks were collected whenever possible, usually a few times each summer. MacroRhizons (Rhizosphere Research Products; Netherlands) were used at stations that were more saturated, also targeting the upper 30 cm of soils. Both techniques were used at stations of intermediate saturation, where both could be deployed effectively. MacroRhizons represent a relatively discrete temporal sampling event (minutes to hours), whereas wicks represent a cumulative water collected over longer periods (weeks to months). It is in this sense, that the two techniques are complimentary. Unfortunately, due to saturation variability both techniques could not be used at all stations and conditions at some Kougarok stations were sometimes too dry to collect meaningful volumes of SPW using either method. Additional SPW data from Kougarok were supplemented from a separate study focused on alder-related nutrient dynamics (McCaully et al., 2022). These data were collected by MacroRhizons and are captured as Kougarok Stations 10 – 13, which were not part of the original stations established by the NGEE Arctic Program. A total of 309 SPW samples from Kougarok were collected and analysed, whereas a total of 89 SPW samples from Teller were collected and analysed.

After collection, SPW cation concentrations were measured in triplicate by inductively coupled plasma optical emission spectroscopy (Optima 2100 DV; PerkinElmer, USA) following US EPA Method 200.7. Inorganic anion concentrations were measured by ion chromatography (DX-600; Dionex, USA) following US EPA Method 300.0. B, F, K, Na, and Si concentrations collected by wicks were excluded from the dataset due to known issues with these ions leeching from fiberglass wick samplers (Perdrial et al., 2014; Wallenberger and Bingham, 2009). This effect is illustrated in **Supplementary Figure 1** and the lack of such an effect for divalent cations is shown in **Supplementary Figure 2**. Comparison of data from wicks and MacroRhizons, along with the observations from (Perdrial et al., 2014), demonstrates that remaining constituents discussed herein were not affected by collection with fiberglass wicks. Alkalinity, pH, and E_H are all critical geochemical parameters that are susceptible to change during storage (Petrone et al., 2007); because of the large amount of data from wicks these parameters were not considered further, except in the context of thermodynamic modelling.

Observations related to vegetation, soil moisture, and permafrost extend were compiled from datasets made available by the NGEE Arctic project and are given for Teller in **Table 1** and for Kougarok in **Table 2**. The reported soil moisture contents were derived from an average of gravimetric measurements (2017 and 2018) and time domain reflectometry measurements (2017 and 2019), and from remotely-sensed P-band Synthetic Aperture Radar (2017). End-of-winter snow depths were measured in March and April of 2016, 2017, and 2018. The annual average ground temperature was measured using in-situ temperature sensors (HOBO U30 DataLogger) at a depth of 1.5 meters below the ground surface (Romanovsky et al., 2020a; Romanovsky, Cable, and Dolgikh, 2020b) and the active layer thicknesses were determined by frost probe in September 2019 at the end of the growing season. Vegetation data were collected at the peak of the growing season in mid to late July 2016 and 2017 at the NGEE Arctic Kougarok and Teller field sites, respectively. The distribution of plant communities in the Arctic is primarily controlled by landscape, topography, soil chemistry, soil moisture, and the plants that historically colonized an area (Raynolds et al., 2019).

184   Soil available rooting depth, which can be limited by shallow depths to bedrock, permafrost, or the water table, can
185   also restrict plant growth and survival of certain species by reducing access to water and nutrients. We surveyed the
186   dominant plant communities along each hillslope, which varied in their shrub abundance, canopy height, and structure,
187   to characterize the vegetation composition at the sites following the recommended protocol of Walker et al. (2016).
188   Extensive field site details and vegetation sampling methods are more thoroughly described in previous studies
189   (Salmon et al., 2019; Langford et al., 2019; Yang et al., 2020; Sulman et al., 2021; Yang et al. 2021).

190   For this study, we provide summary statistics for vegetation plots associated with intensive stations. Vegetation
191   composition plots within each intensive station were chosen subjectively in areas of homogeneous and representative
192   vegetation varying in size from 1 to 25 m^2 depending on canopy structure and height. The surveyed plot area was 1 ×
193   1 m for all plant communities except for the taller stature willow-birch tundra, mesic willow shrubland (2.5 × 2.5 m),
194   and alder shrubland (5 × 5 m). For each plot, all plant species (vascular plants, lichens, and bryophytes) were recorded
195   along with visual estimates of their percent cover. For plots with multiple canopies, field cover estimates were recorded
196   as absolute cover, meaning that the total cover per plot can be >100%. We calculated relative cover values (adding to
197   100%) from the field data and use these for all subsequent analyses.

198   Plant species were further aggregated into nine plant functional types (PFTs), groupings of plant species that share
199   similar growth forms and roles in ecosystem function (Wullschleger et al., 2014), based on growth patterns and plant
200   traits. PFTs in this study include: (1) nonvascular mosses and lichens, (2) deciduous and evergreen shrubs of various
201   height classes, including an alder PFT, (3) graminoids, and (4) forbs. Photos of representative PFTs from both sites
202   are given in **Supplementary Figures 9-17**. Canopy height was estimated within each plot for each PFT as the average
203   of 4 measurements, including a maximum canopy height. Active layer depth was measured at the end of the growing
204   season for all plots in September 2018 using a frost probe. A temperature probe was used to determine if the resistive
205   layer was permafrost (≤0 °C) or rock (>2 °C). Thaw depth is an average of 4 measurements from the vegetation plot
206   corners.

2.3 Statistical Analysis

208   Principal Components Analysis (PCA) and the Mann-Whitney U-Test (MWUT) were both used to investigate
209   dominant environmental controls on solute concentrations in SPWs at Teller and Kougarok. PCA is an exploratory
210   data analysis tool that reduces the dimensionality of large complex datasets and considers how components (i.e. solute
211   concentrations) vary together. Because PCA was predominately used as a screening tool to reveal geochemical
212   correlations that may not have been evident by traditional geochemical causations or inference, a detailed discussion
213   of the PCA results is reserved to the Supplementary Materials. The MWUT was used to test for significant differences
214   in solute concentrations between Teller and Kougarok (inter-site variability) and between stations at each site (intra-
215   site variability). The MWUT is a non-parametric method of challenging a null hypothesis, which in this case is the
216   assumption that the concentrations of a given solute are not systematically greater at either site nor at any particular
217   station. Water chemistry data are typically not normally distributed and thus, non-parametric difference tests such as
218   the MWUT are preferred. The MWUT challenges the distribution of values, not the means. In this work, the level of
219   significance associated with the null hypothesis was operationally defined as 0.05, which equates to a 95 % chance

220 that an observed statistical difference is real and not coincidental. This error rate is operationally defined per contrast

221 (i.e. a 95 % chance that the observed statistical difference in nitrate concentrations between Teller Station 9 and Teller

222 Station 7 is real or that the observed statistical difference in sulphate concentrations between Teller and Kougarok is

223 real) as opposed to familywise (i.e. a 95 % chance that all of the observed/reported statistical differences are real and

224 not coincidental). MWUTs were completed using the methods described in Corder and Foreman (2009) and PCA was

225 completed using packages available in R statistical software, version 3.3.6 (Corder and Foreman, 2009; R Core Team,

226 2020). For all analyses, concentrations below the method detection limit were operationally defined as half the

227 detection limit, in agreeance with (Helsel, 2005, p. 43). While the emphasis of this study was on site/station (i.e.

228 spatial) variability, it should be recognized that seasonal and inter-annual variability could also be significant. To

229 minimize seasonal forcing on the variability observed, all SPW geochemical data presented were collected during the

230 thaw season between June and September.

231 **2.4 Thermodynamic Modelling**

232 To investigate thermodynamic controls on solute behaviour, particularly solubility limitations, thermodynamic

233 modelling exercises were undertaken using PHREEQC, a thermodynamic geochemical modelling code, and

234 PhreePlot, which facilitates repetitive PHREEQC calculations through looping (Kinniburgh and Cooper, 2011;

235 Parkhurst and Appelo, 2013). Because this study was focused on elucidating the primary geochemical controls on

236 solute concentrations in SPWs and not on developing a rigorous transport model, representative concentrations were

237 used instead of station specific concentrations. Representative "low", "median", and "high" concentration conditions

238 were proxied from the 25th, 50th, and 100th concentration percentiles, respectively, taken from both Teller and

239 Kougarok (Supplementary **Table 4**). Meanwhile, representative pH and E_H ranges were determined either through

240 direct measurement (pH), or indirectly by correlating dissolved Fe^{2+} concentrations and pH with a redox condition

241 through geochemical models and the Nernst equation. Modelling exercises were performed utilizing the phreeqc.dat

242 database, with the only modification being the suppression of methane production by inorganic carbonate reduction.

243 Modelling exercises were performed at the default PHREEQC modelling temperature (25 °C), as the selection of an

244 alternative defensible temperature was non-trivial; temperatures on the Seward Peninsula span a very wide range and

245 its unclear what temperature would be most suitable for mineral solubility limitation modelling. Ultimately, because

246 the thermodynamic models were used as a tool understand what could be controlling soil pore water solute

247 concentrations and were not intended to model the system or to predict future concentrations, the default temperature

248 was decided to be the most suitable. While there is some temperature dependence of mineral solubility, the differences

249 in predicted solubility between 4 °C and 25 °C did not impact the interpretation of our results (**Supplementary Figure**

250 **8**). Methane production was "turned-off" to maintain carbonate availability under reducing conditions to help identify

251 any possible carbonate minerals that could be precipitating. Because alkalinity was only measured in a small number

252 of samples, carbonate concentration percentiles were estimated from charge imbalances. Alkalinity and charge

253 imbalance were very well correlated in samples where alkalinity was measured (**Supplementary Figure 3**). Although

254 not a particularly rigorous modelling exercise, this approach was sufficient to identify mineral phases that could be

255 controlling solute generation processes through solubility limitations.

3. Results

3.1 Physical Characteristics of Stations (Co-Located Studies)

Controls on the observed spatial variability of SWP solute concentrations at Teller and Kougarok stations were deduced, in part, from differences in physical features and conditions of each station. Quantitative measures of many of these physical characteristics were available from the interdisciplinary studies co-located at the Teller and Kougarok stations. The extent of permafrost, ground temperature, active layer depth, soil moisture content, snow depth, vegetation type, vegetation canopy height, dominant plant functional type, and hillslope position were all complied from these co-located studies. Using these measures, the physical characteristics of each station are summarized in **Table 1** and **Table 2**, grouped by vegetation type.

3.2 Inter-site Variability: Teller versus Kougarok

Mann-Whitney U-Testing revealed that the concentrations of 14 of the 23 constituents analysed were significantly different ($1.96 < |z|$) between Teller and Kougarok (**Table 3**). The effect size, a measure of how significantly different the concentrations were, were large for Na and F; medium-large for K and Si; medium for Al, Oxalate, B, Zn, SO_4^{2-}, Fe, Ba, Ti, and NO_2^-; and small-medium for Li. The terminology and thresholds for these semi-quantitative differences in correlation were taken from Corder and Foreman (2009). Mann-Whitney U-testing revealed that SPW concentrations of many constituents were significantly different between Teller and Kougarok (**Table 3**). When concentrations were significantly different between the sites, Kougarok generally exhibited the higher concentrations of the two. SPW concentrations of Na, F, K, Si, Al, oxalate, B, Zn, Fe, Ba, Ti, NO2, and Li were all significantly greater at Kougarok than Teller, while only SO_4^{2-} concentrations were significantly greater at Teller. Meanwhile, the concentrations of Br, NO_3^-, Sr, PO4, Mg, Cr, Mn, Cl, and Ca were not significantly different between Teller and Kougarok. A summary of the inter-site MWUT results are given in **Table 3** with the constituents that exhibited significant differences between the sites displayed over a darkened background.

3.3 Intra-site Variability: Teller and Kougarok Stations

Mann-Whitney U-Testing was also used to test for intra-site differences between stations at both Teller and Kougarok. Boxplots and compact letter displays are used to visualize the within-site variability of a select group of constituents of interest (COIs), which are given in **Figure 4**. Tables of the results of the intra-site MWUTs for all constituents that were monitored, including those that did not demonstrate some systematic inter-station variability or were not otherwise of interest, are given in the Supplementary Materials. Our interpretation of the major environmental controls on the observed spatial variability of SPW solute concentrations between stations are shown in **Table 4**. Each of these controls, including vegetation effects, soil moisture and redox effects, weathering, water/soil interactions and hydrological transport effects, and mineral solubility effects, is considered in detail in the following sections.

3.3.1 Vegetation Effects

Vegetation can influence hydrogeochemical variability directly via vegetation-induced changes to elemental cycling and soil moisture contents, or indirectly via the secondary impacts changes in soil moisture can have on mineral

290   solubility or on the soil redox condition. The geochemical consequences of solubility and redox conditions are the
291   focus of sections to follow, thus, this section will focus on direct vegetation effects via influences on elemental cycling
292   and soil moisture via evapotranspiration and preferential trapping of snow.

293   NO_3^- was the only COI that showed a distinct effect from vegetation via elemental cycling. Elevated NO_3^-
294   concentrations were associated with the presence of alder shrubs and, in some cases, willow shrubs. NO_3^-
295   concentrations at both sites were generally low, with the exception of Kougarok Stations 3, 5, and 12, and Teller
296   Station 7 (**Figure 4**). Low to tall alder shrubs are the dominant vegetation type at Kougarok Stations 3 and 12 (**Table
297   2**). Meanwhile, alders are present at Kougarok Station 5 despite the dominant vegetation type being low willow and
298   birch shrubs. Alders increase soil nitrogen through a symbiotic relationship with nitrogen-fixing bacteria that reside
299   in their root nodules, thus, an association between NO_3^- concentrations and alder vegetation is expected (Salmon et
300   al., 2019).

301   Perhaps more noteworthy was the lack of elevated NO_3^- concentrations at Kougarok Stations 1, 2, 6, 10, and 11. The
302   vegetation type at Kougarok Stations 1, 2, 6, 10, and 11 is alder savanna in tussock tundra, which is a mixed graminoid-
303   shrub tundra with shorter stature and lower density of alder shrubs, yet nonetheless nitrogen input via alder derived
304   nitrogen-fixation is anticipated to occur. The lack of elevated NO_3^- suggests either that 1) nitrogen-fixation in alder
305   savanna in tussock tundra is insufficient to result in an increase in NO_3^- concentrations, 2) that the Kougarok footslope
306   and lower backslope is very nitrogen-limited, and thus, that NO_3^- is largely consumed by vegetation as it is fixed, or
307   3) that microbes in the Kougarok footslope and lower backslope rapidly denitrify the available NO_3^- as a substitute
308   for oxygen in their metabolisms. The smaller shrub size and density in the alder savanna in tussock tundra certainly
309   results in less accumulated leaf litter relative to the denser and larger alder shrubland intensive stations, as such, it
310   seems reasonable that less nitrogen would be available at stations in alder savanna in tussock tundra. Meanwhile,
311   isotopic measurements of nitrogen downslope of alder patches at Kougarok Stations 12 and 3 also support the
312   occurrence of denitrification (McCaully et al., 2022). Therefore, we believe the lack of elevated NO_3^- concentrations
313   at Kougarok Stations 1, 2, 6, 10, and 11 is a combination of less alder leaf litter and greater denitrification, than at
314   Kougarok Stations 3, 5, or 12.

315   At Teller, only Station 7 exhibited elevated NO_3^- concentrations relative to the rest of the catchment (**Figure 4**). Teller
316   Station 7 is dominated by tall willow shrubs and is relatively dry. Mineralization and nitrification of willow leaf litter
317   coupled with limited microbial denitrification is the presumed cause of elevated NO_3^- concentrations at Teller Station
318   7. Teller Station 2 also has tall willow shrubs but did not exhibit elevated NO_3^- concentrations. From the limited scope
319   of this study, it is unclear why Teller Station 2 did not exhibit elevated NO_3^- while Station 7 did, but we suspect that
320   higher seasonal moisture content and greater microbial denitrification at Teller Station 2 likely played a role. Also of
321   note was that despite significant intra-site NO_3^- concentration differences, inter-site differences were not significant
322   ($|z| = 1.59$) and that relatively few Kougarok stations showed elevated NO_3^- concentrations, despite a widespread alder
323   presence. Increased microbial denitrification is suspected to balance increased nitrogen-fixation at these stations. This
324   is consistent with previous studies that have noted higher nitrogen mineralization rates in acidic tundra than non-acidic
325   tundra (Weiss et al., 2005); Kougarok is predominantly acidic tundra and Teller is non-acidic tundra.

The effect of vegetation on spatial variability of soil moisture was not readily observed in the volumetric moisture content of soil (**Table 1** and **Table 2**) but was somewhat apparent in the spatial variability of moisture sensitive constituents, such as Cl (**Figure 4**). The lack of a clear correlation between vegetation and soil moisture by TDR or P-band SAR observations is perhaps do to the coarseness of the P-band SAR observations and the strong seasonality associated with both methods. Moisture sensitive constituents, such as Cl, may provide a more seasonally averaged tracer of soil moisture content at the stations. An increase in Cl concentrations with vegetation canopy height was apparent at Teller stations suggesting an evapotranspiration effect. This trend was also apparent at Kougarok, but the differences were rarely significant. Overall, the spatial variability of soil moisture sensitive constituents, like Cl, was far less correlated with vegetation-type than expected; perhaps due to preferential trapping of snow, which may offset the increased evapotranspiration of tall shrubs more than previously realized. Overall, Cl concentrations at Kougarok appeared to be more correlated with hillslope position than with vegetation canopy height (**Figure 4**).

3.3.2 Soil Moisture and Redox Effects

Soil moisture content can have a profound effect on redox sensitive elements. Saturation limits oxygen diffusion into soil, and thus, forces microorganisms to utilize less energetic electron acceptors to metabolize organic matter. In an ideal system, soil microorganisms will use the strongest electron acceptor available, until it is exhausted. Although natural environments are not ideal systems, redox conditions in soils follow a more or less stepwise progression. Therefore, by evaluating the dissolved concentrations of NO_3^-, Mn, Fe, and SO_4^{2-} in SPWs, it is possible to qualitatively assess soil redox conditions and their impact on hydrogeochemical variability.

The redox conditions at both Teller and Kougarok are generally limited by Fe reduction, with the most reducing conditions found at stations with the highest soil moisture content. As such, NO_3^- concentrations are generally low (**Table 3**), SO_4^{2-} concentrations are relatively consistent (**Figure 4**), and Mn and Fe concentrations increase with increasing soil moisture (**Figure 4**). NO_3^- concentrations were generally low, except for drier stations in the proximity of tall alders or willows. While NO_3^- inputs are discussed in the vegetation effects section, the lack of high NO_3^- concentrations at wetter stations that contain alders suggests that soil moisture coupled with microbial denitrification bares a strong control on SPW NO_3^- concentrations. Meanwhile, SO_4^{2-} concentrations at both sites are relatively constant across clear moisture and redox gradients (**Figure 4**). This suggests that SO_4^{2-} reduction is not pervasive at either site. Dissolved Fe concentrations were higher at stations with higher soil moisture content, consistent with Fe reduction. Similarly, Mn concentrations were slightly elevated at wetter stations. The concentrations of Mn, however, rarely rose above 0.05 mg·L 1, suggesting either Mn solubility limitations or a lack of a significant Mn weathering source. Low Mn concentrations at Teller Station 5, a wetter station on the upper shoulder of the Teller watershed (**Table 1**; **Figure 2**) seems to support the latter conclusion, as do geochemical modelling exercises (Section 4.5). Together, these results suggest that the most reducing condition at both sites is typically limited to Fe reduction and that this only occurs at stations with the highest soil moisture contents.

3.3.3 Weathering, Water/Soil Interaction, and Hydrological Transport Effects

A combination of weathering, water/soil interactions, and hydrological transport were identified as probable drivers of hydrogeochemical variability for some solutes. As noted by Philben et al. (2020), soil derived solutes tend to accumulate in low-lying areas within watersheds. This is observed at Teller, where the concentrations of Ca, Sr, and Mg all increase dramatically at the transition from lower backslope to footslope (**Figure 5**). Both Teller and Kougarok are underlain by carbonate-rich metamorphic facies, and Ca, Sr, and Mg are probable carbonate counter-cations. Weathering of Ca, Sr, and Mg carbonates and subsequent transport of these cations downslope explains this pattern of spatial variability. At Kougarok, concentrations of Ca, Mg, and Sr similarly increase from upper backslope to footslope, but concentrations of Ca and Sr decrease further down the lower backslope (Stations 10 and 1), while Mg concentrations continue to increase. A possible explanation for this behaviour is the greater affinity of cation exchange surfaces for Ca and Sr compared to Mg, thus, Ca and Sr are preferentially retained in the footslope whilst Mg is transported further down the lower backslope (Sparks, 2003, p. 189).

3.3.4 Mineral Solubility Effects

Although redox reactions are rarely at equilibrium in natural environments, comparison of field data with equilibrium models provides valuable semi-quantitative insight into the redox condition of natural environments. Because Fe appeared to be limiting the development of more reducing conditions (Section 4.3), select samples from both sites were measured for soluble Fe^{2+} following methods presented in Viollier et al. (2000). These concentrations of aqueous Fe^{2+} were then compared with model-predicted concentrations of Fe^{2+}, when coupled with an infinite $Fe(OH)_{3(am)}$ phase, across a range of pH values (2 – 10) and fixed E_H values of 400 mV, 200 mV, 0 mV, and -200 mV; activity coefficients were assumed to be equal to 1. The measured and modelled Fe^{2+} concentrations are compared in **Figure 6**, where concentrations that were below the method detection limit (0.05 mg·L-1) are set equal to 0.025 mg·L-1 (half the detection limit). Comparison of model predicted Fe^{2+} concentrations with field data suggests that while Teller exhibits a narrower range of pH conditions than Kougarok, it exhibits a broader range of redox conditions (**Figure 6**). Although several Fe^{2+} measurements were below the detection limit, suggesting oxidizing conditions, high Fe^{2+} concentrations in some samples suggested E_H values below 0 mV. Therefore, Fe redox conditions at Teller ranged from mildly reducing to oxic and Fe redox conditions at Kougarok ranged from mildly oxic to oxic. Oxidation-reduction potentials (ORPs), calculated from pH, Fe^{2+} concentrations, and the Nernst equation suggest that ORPs at Teller were as low as - 69 mV, while the lowest ORP at Kougarok was + 134 mV (**Figure 6**). Maximum ORP values could not be determined quantitatively as some Fe^{2+} concentrations were below Fe^{2+} detection limits, at both sites.

E_H/pH predominance diagrams were created from the 25th, 50th, and 100th concentration percentiles and are shown in **Figure 7** for the COIs where precipitation of mineral phases were predicted under some conditions. The concentrations for these diagrams were taken from filtered aqueous concentration data, thus, predicted mineral precipitation is an indication of nearly saturated or over-saturated conditions. The range of E_H and pH conditions observed at Teller and Kougarok are overlaid as solid yellow and solid blue lines, respectively. Only the predominance diagrams that indicated possible mineral formation under the E_H/pH conditions present at either site are shown in **Figure 7**. These phases included $Fe(OH)_{3(am)}$ (Fe), siderite (Fe), $Al(OH)_{3(am)}$ (Al), chalcedony (Si), barite (Ba and

395 SO_4), calcite (Ca), dolomite (Ca and Mg), and rhodochrosite (Mn). Predominance diagrams for the remaining key

396 COIs that were not predicted to form any mineral phases under any site conditions are given in **Supplementary Figure**

397 **4**.

398 To further examine which mineral phases could be controlling SPW solute concentrations, saturated conditions for

399 the mineral phases identified in **Figure 7** were modelled using sweeps of pH values from 2 – 10 at various fixed E_H

400 values (400mV, 200mV, 0mV, and -200mV). Predicted solute concentrations under the modelled saturated conditions

401 were then compared with field data to find common trends. In general, if solute concentrations were frequently

402 measured near the saturation of a mineral, or were identified to have similar dependence on pH or E_H, it was inferred

403 that the mineral phase could be controlling the generation of that solute. The mineral phases that were identified to

404 possibly be controlling solute concentrations were $Al(OH)_{3(am)}$, $Fe(OH)_{3(am)}$, chalcedony, and barite. This does not

405 preclude the presence of significant concentrations of other mineral phases, it only identifies these as possibly

406 controlling the dissolved concentrations of Al, Fe, Si, and Ba, respectively. Although it does not provide mineralogical

407 information, X-ray fluorescence (XRF) data reported by another study at Teller confirmed high concentrations of Al,

408 Fe, Si, and Ba in the organic and mineral soil layers at that site (Graham et al., 2018). We are unaware of any similar

409 studies at Kougarok, nor are we aware of any studies that provide would provide confirmatory mineralogical

410 information, for example by X-ray diffraction (XRD).

411 Aluminium concentrations in SPWs at both Teller and Kougarok appear to be controlled by the

412 dissolution/precipitation of amorphous Al hydroxide ($Al(OH)_{3(am)}$) (**Figure 8**). The solubility limit of $Al(OH)_{3(am)}$ has

413 no redox dependence, but is highly pH dependent. Aluminium concentrations were generally clustered near the

414 solubility limit of $Al(OH)_{3(am)}$; $Al(OH)_{3(am)} + 3H^+ \leftrightarrow Al^{3+} + 3H_2O$; log k = 10.8. This suggests that Al SPW

415 concentrations at both sites are controlled by wetting/drying (dissolution/precipitation) processes. It also suggests that

416 there could be a significant amount of $Al(OH)_{3(am)}$ in the soils at both sites. While organic matter may also sorb to

417 alumina surfaces, the adherence to the solubility of $Al(OH)_{3(am)}$ suggests that significant concentrations of Al are not

418 complexed with dissolved organic matter. The predominance diagrams highlight 1) the strong pH dependence on the

419 stability of $Al(OH)_{3(am)}$, 2) the influence of dissolved F can have on Al speciation when Al concentrations are low,

420 and 3) that Al is a cation at low pH and an anion at high pH (**Figure 7**). Despite being a weathering product, Al

421 concentrations show a dissimilar downslope trend to other weathering products, especially at Teller (**Supplementary**

422 **Figure 5**). While the concentrations of weathering products generally increase with distance downslope, Al

423 concentrations decrease. We suspect this can be attributed to increasing pH with distance downslope. Philben et al.

424 (2020) reported a 1 pH unit increase in pH in organic soils along the Teller transect (**Figure 2**), increasing from 5.6 at

425 Station 5 to 6.7 at Station 9. Such an increase would decrease the solubility of $Al(OH)_{3(am)}$, and thus, decrease the

426 concentration of dissolved Al (**Figure 8**).

427 Similar to Al, Fe concentrations in SPWs at both Teller and Kougarok appear to be controlled by the

428 dissolution/precipitation of amorphous Fe hydroxide ($Fe(OH)_{3(am)}$). Fe concentrations were generally clustered near

429 the solubility limit of $Fe(OH)_{3(am)}$ (**Figure 8**). Unlike $Al(OH)_{3(am)}$ however, $Fe(OH)_{3(am)}$ solubility is dependent on the

430 redox condition in addition to the pH; $Fe(OH)_{3(am)} + 3H^+ + e- \leftrightarrow Fe^{2+} + 3H_2O$; log k = 16.0 (**Figure 8**). Fe(III) is only

431 sparingly soluble in aqueous solutions and reduction to Fe(II) significantly increases the solubility of Fe, thus, at a

432   given pH value higher aqueous concentrations are predicted and observed under more reducing conditions (**Figure 8**).

433   Iron concentrations in SPWs at both sites generally follow the pH dependence of $Fe(OH)_{3(am)}$ solubility (**Figure 8**).

434   This suggests that SPW concentrations of Fe at both sites are controlled by wetting/drying (dissolution/precipitation)

435   processes, coupled with the redox condition.

436   Si concentrations are frequently limited by the solubility of chalcedony, a very finely grained form of SiO_2, which is

437   much more soluble than quartz; $SiO_2 + 2H_2O \leftrightarrow H_4SiO_4$; log k = - 3.55. Particularly at Kougarok, the dissolved Si

438   concentrations, coupled with a lack of a strong pH or E_H dependence, suggest a controlling influence of chalcedony.

439   Ba concentrations also appear to be controlled by solubility, but rather than by the solubility of an oxide or a hydroxide

440   phase, by the solubility of barite $[Ba^{2+} + SO_4^{2-} \leftrightarrow BaSO_4(s)$; log k = 9.97]. Unlike Al hydroxide or Fe hydroxide, barite

441   solubility lacks a strong pH dependence and instead is dependent solely on the activities of Ba^{2+} and SO_4^{2-}. Unlike Ba,

442   SO_4^{2-} concentrations are not limited by the solubility limit of barite and are generally higher and not well correlated

443   with Ba concentrations. Together, these suggest that SO_4^{2-} from another source (likely, atmospheric deposition or

444   sulfidic mineral oxidation), is suppressing barite dissolution, and thus, is reducing dissolved Ba concentrations. Barite

445   solubility can exhibit a redox dependence if conditions are sufficiently reducing to reduce SO_4^{2-} to sulphide. This shifts

446   the equilibrium to greater dissolution of barite, and therefore higher conditions of Ba. The lack of E_H dependence in

447   observational data further suggests that neither site exhibits significant SO_4^{2-} reduction.

448   **4. Discussion**

449   The 18 stations examined herein (8 at Teller and 10 at Kougarok) represent a wide range of vegetation types, soil

450   moisture contents, permafrost extents, and hillslope positions. Coupling the spatial variability of these landscape

451   characteristics with the spatial variability of SPW solute concentrations provides valuable insight into the dominant

452   environmental controls on observed spatial variability of SPW geochemistry. It is our hope that correlating SPW

453   geochemistry with readily observable and scalable landscape features will inform earth system modelling efforts in

454   permafrost regions and provide fast and easy methods to determine if earth system models are working properly (i.e.

455   predicting the correct trends). The inferred dominant environmental controls on the observed inter-site and intra-site

456   variability of SPW solute concentrations are discussion in the following sections.

457   **4.1 The Dominant Environmental Controls on Inter-site Variability of SPW Solute Concentrations**

458   Overall, the more frequent instance of significantly greater constituent concentrations at Kougarok suggests a

459   systematic cause. The extensive low-gradient toeslope (**Figure 2**) and lack of a well-defined drainage channel at

460   Kougarok, are likely causes of the systematically higher SPW solute concentrations at Kougarok. Water perching, the

461   result of near-surface permafrost in the lower-backslope and toeslope, increases evapotranspiration and, thus, SPW

462   solute concentrations. Meanwhile, the lack of a drainage channel at Kougarok suggests that runoff (and therefore

463   solute exports) is more limited than at Teller. Without a relatively rapid export mechanism such as a stream channel,

464   solute transport is likely limited to interflow within the Kougarok hillslope over much of the thaw season, allowing

465   weathering products to increase to significantly greater concentrations than those observed at Teller, where a well-

466 defined drainage/export mechanism does exist. Field observations from pits at Kougarok confirm observable interflow
467 at the site. Overall, our study suggests that evaporative concentration could be a significant control on SPW solute
468 concentrations in permafrost catchments, especially in those with limited drainage and therefore a perched near-
469 surface water table. This effect has been reported previously (Raudina et al., 2017), but does not appear to be widely
470 considered, perhaps due to the generally few studies of SPW solutes in permafrost regions. We suggest future efforts
471 to predict future SPW solute and nutrient dynamics directly address the impacts of evaporative concentration on
472 permafrost catchments, especially with future permafrost thaw.

473 The exception to the general observation of elevated concentrations at Kougarok versus Teller was SO_4^{2-}. Although
474 the cause of consistently higher SO_4^{2-} concentrations at Teller is unclear from the limited scope of this study, it seems
475 likely to be due to a greater abundance of sulfidic bedrock material. The presence of sulfidic bedrock in the vicinity
476 of Teller has been reported by mineral prospecting efforts (Brobst, Pinckney, and Sainsbury, 1971; Herreid, 1966;
477 Mulligan, 1965); we are unaware of any such reports near Kougarok.

478 **4.2 The Dominant Environmental Controls on Intra-site Spatial Variability of SPW Solute Concentrations**

479 Vegetation influences on elemental cycles were only readily apparent for nitrogen and although vegetation induced
480 changes to soil moisture content were discernible, they were far less significant than anticipated. NO_3^- was the only
481 COI that exhibited a clear vegetation effect; elevated concentrations were associated with the presence of alder shrubs
482 and, in some cases, tall willow shrubs. These increases in NO_3^- concentrations associated with alder nitrogen-fixation
483 and the mineralization and nitrification of willow leaf litter were frequently equipoised by increased microbial
484 denitrification in regions sufficiently moist to support it, this is perhaps one of the most significant finding of this
485 work. Although both Kougarok and Teller exhibited some indications of increased Cl concentrations in the presence
486 of tall shrubs, the net vegetation effect on soil moisture was far less than hypothesized. Redox sensitivity was also less
487 then hypothesized and most stations seemed well-buffered at Fe redox conditions. The result of this buffering was
488 generally low NO_3^- concentrations (except where vegetation effects dominated), consistent SO_4^{2-} concentrations across
489 clear redox gradients, and variable Mn and Fe concentrations. Mn concentrations were generally low, likely due to a
490 limited source. Fe concentrations were higher at stations with higher soil moisture content, consistent with Fe
491 reduction. Similar Fe redox cycling between soluble Fe(II) species and precipitated Fe oxyhydroxides in permafrost
492 catchments has been reported recently (Patzner et al., 2022), which suggests that Fe redox buffering in permafrost
493 landscapes is widespread. Weathering, water/soil interactions, and hydrological transport were probable drivers of
494 variability for Ca, Sr, and Mg. Ca, Sr, and Mg all tended to accumulate in low-lying areas, although Ca and Sr
495 demonstrated greater accumulation potential than Mg, likely via greater affinity of cation exchange surfaces for Ca
496 and Sr compared to Mg. Mineral solubility limitations were the primary controls on Al ($Al(OH)_{3(am)}$), Fe ($Fe(OH)_{3(am)}$),
497 Ba (barite), and Si (chalcedony) concentrations. This suggests that the SPW concentrations of these constituents will
498 remain stable until those mineral phases are exhausted or soil pore hydrochemistry changes sufficiently to alter the
499 solubility of those mineral phases. Supersaturation of Al with respect to gibbsite (crystalline $Al(OH)_3$) and Si with
500 respect to chalcedony in a permafrost wetland has been reported previously (Jesson et al., 2014). The solubility curves
501 for gibbsite and $Al(OH)_{3(am)}$ are similar, with $Al(OH)_{3(am)}$ being slightly more soluble at all pH values do to the

increased thermodynamic stability of the crystalline Al hydroxide mineral, gibbsite. Meanwhile, seasonal precipitation of Fe oxyhydroxides in permafrost peatlands and their effect of carbon cycling was the subject of an excellent paper by Patzner et al. (2022). Our study is the first observation we are aware of the saturation controls of barite on Ba in permafrost SPWs, although that could be because few relatively few studies consider barium concentrations; it is worthwhile noting the Ba was not supersaturated with respect to barite but approached a saturated condition. Future studies should also note that changes in redox condition would significantly alter $Fe(OH)_{3(am)}$ solubility, whereas changes in pH conditions would significantly alter $Al(OH)_{3(am)}$ and $Fe(OH)_{3(am)}$ solubility.

Although discerning the environmental controls on spatial variability of SPW solute concentrations provides some high-level insight into the effects changes in landscape character may have on soil pore hydrochemistry, our scope was limited and leveraged on previously available datasets. The significance of SPW in small Arctic headwater catchments as a key initial component in the freshwater hydrologic continuum is under recognized, and such catchments warrant more detailed and systematic investigations.

5. Acknowledgements

We would like to thank the Sitnasuak Native Corporation and the Mary's Igloo Native Corporation for their guidance and for allowing us to conduct this research on the traditional homelands of the Inupiat people. Funding was provided by the Next-Generation Ecosystem Experiments (NGEE Arctic) project, supported by the Office of Biological and Environmental Research in the U.S. DOE Office of Science. We wish to thank Lauren Charsley-Groffman and Nathan Wales for their assistance with fieldwork, as well as, George Perkins, Oana Marina, Rose Harris, and Emily Kluk for their assistance with laboratory analyses.

6. Data availability statement

The data that support the findings of this study are made openly available in the NGEE-Arctic data repository at (DOI: 10.5440/1735757).

7. References

Anderson, M. D., Ruess, R. W., Myrold, D. D., and Taylor, D. L. (2009). Host species and habitat affect nodulation by specific Frankia genotypes in two species of Alnus in interior Alaska. Oecologia 160, 619–630. doi: 10.1007/s00442-009-1330-0

Anderson, M. D., Ruess, R. W., Uliassi, D. D., and Mitchell, J. S. (2004). Estimating N2 fixation in two species of Alnus in interior Alaska using acetylene reduction and 15N2 uptake. Ecoscience 11, 102–112. doi: 10.1080/ 11956860.2004.11682814

Binkley, D., Sollins, P., Bell, R., Sachs, D., and Myrold, D.: Biogeochemistry of adjacent conifer and alder-conifer stands, Ecology, 73, 2022–2033, 1992.

Breen, A., Iversen, C., Salmon, V., VanderStel, H., Busey, B., and Wullschleger, S. 2020a:. NGEE Arctic Plant Traits: Plant Community Composition, Kougarok Road Mile Marker 64, Seward Peninsula, Alaska, 2016 [Data set], doi: https://doi.org/10.5440/1465967.

Breen, A., Iversen, C., Salmon, V., VanderStel, H., Busey, B., and Wullschleger, S. 2020b:. NGEE Arctic Plant Traits: Plant Community Composition, Kougarok Road Mile Marker 64, Seward Peninsula, Alaska, 2016 [Data set], doi: https://doi.org/10.5440/1465967.

Bring, A., Fedorova, I., Dibike, Y., Hinzman, L., Mård, J., Mernild, S. H., … Woo, M.-K. 2016: Arctic terrestrial hydrology: A synthesis of processes, regional effects, and research challenges. Journal of Geophysical Research: Biogeosciences, 121: 621–649, doi: https://doi.org/10.1002/2015JG003131.

Brobst, D. A., Pinckney, D. M., and Sainsbury, C. L. 1971: Geology and Geochemistry of the Sinuk River Barite Deposit, Seward Peninsula, Alaska (No. 463 (?)). United States Department of the Interior Geological Survey.

Bühlmann, T., Hiltbrunner, E., and Körner, C.: Alnus viridis expansion contributes to excess reactive nitrogen release, reduces biodiversity and constrains forest succession in the Alps, Alpine Botany, 124, 187–191, https://doi.org/10.1007/s00035-014-0134-y, 2014.

Clein, J. S. and Schimel, J. P.: Nitrogen turnover and availability during succession from alder to poplar in Alaskan taiga forests, Soil Biology and Biochemistry, 27, 743–752, https://doi.org/10.1016/0038-0717(94)00232-P, 1995.

Conroy, N., Heikoop, J., Newman, B., Wilson, C., Arendt, C., Perkins, G., and Wullschleger, S. 2021: Soil Water Chemistry and Water and Nitrogen Isotopes, Teller Road Site and Kougarok Hillslope, Seward Peninsula, Alaska, 2016 - 2019 [Data set], doi: https://doi.org/10.5440/1735757.

Corder, G. W., and Foreman, D. I. 2009: Nonparametric statistics for non-statisticians: a step-by-step approach. Hoboken, N.J:, Wiley, 247 pp.

Frey, K. E., and McClelland, J. W. 2009: Impacts of permafrost degradation on arctic river biogeochemistry. Hydrological Processes, 23: 169–182, doi: https://doi.org/10.1002/hyp.7196.

Frisbee, M. D., Phillips, F. M., Campbell, A. R., and Hendrickx, J. M. H. 2010: Modified passive capillary samplers for collecting samples of snowmelt infiltration for stable isotope analysis in remote, seasonally inaccessible watersheds 1: laboratory evaluation. Hydrological Processes, 24: 825–833, doi: https://doi.org/10.1002/hyp.7523.

Fuchs, M., Nitze, I., Strauss, J., Günther, F., Wetterich, S., Kizyakov, A., … Grosse, G. 2020: Rapid Fluvio-Thermal Erosion of a Yedoma Permafrost Cliff in the Lena River Delta. Frontiers in Earth Science, 8: 336, doi: https://doi.org/10.3389/feart.2020.00336.

Graham, D. E., Kholodov, A., Wilson, C. J., Moon, J.-W., Romanovsky, V. E., and Busey, B. 2018: Soil Physical, Chemical, and Thermal Characterization, Teller Road Site, Seward Peninsula, Alaska, 2016., doi: https://doi.org/10.5440/1342956.

Harms, T. K., and Jones, J. B. 2012: Thaw depth determines reaction and transport of inorganic nitrogen in valley bottom permafrost soils. Global Change Biology, 18: 2958–2968, doi: https://doi.org/10.1111/j.13652486.2012.02731.x.

Harms, T. K., and Ludwig, S. M. 2016: Retention and removal of nitrogen and phosphorus in saturated soils of arctic hillslopes. Biogeochemistry, 127: 291–304, doi: https://doi.org/10.1007/s10533-016-0181-0.

570   Helsel, D. R. 2005: Nondetects and data analysis: statistics for censored environmental data. Hoboken, NJ:, Wiley-

571   Interscience, 250 pp.

572   Herreid, G. 1966: Preliminary geology and geochemistry of the Sinuk River area. Seward Peninsula, Alaska: Alaska

573   Division of Mines and Minerals Geologic Report, 24: 19.

574   Hiyama, T., Yang, D. and Kane, D.L., 2021. Permafrost Hydrology: Linkages and Feedbacks. In Arctic Hydrology,

575   Permafrost and Ecosystems (pp. 471-491). Springer, Cham.

576   Hollingsworth, T. N., Lloyd, A. H., Nossov, D. R., Ruess, R. W., Charlton, B. A., and Kielland, K. (2010). Twenty-

577   five years of vegetation change along a putative successional chronosequence on the Tanana River, Alaska. *Can. J.*

578   *For. Res.* 40, 1273–1287. doi: 10.1139/X10-094

579   Hopkins, D. M., Karlstrom, T. N. V., Black, R. F., Williams, J. R., Pewe, T. L., Fernald, A. T., and Muller, E. H.

580   1955: Permafrost and ground water in Alaska. U.S. Geological Survey Professional Paper 264-F.

581   Jafarov, E. E., Coon, E. T., Harp, D. R., Wilson, C. J., Painter, S. L., Atchley, A. L., and Romanovsky, V. E. 2018:

582   Modelling the role of preferential snow accumulation in through talik development and hillslope groundwater flow in

583   a transitional permafrost landscape. Environmental Research Letters, 13: 105006, doi: https://doi.org/10.1088/1748-

584   9326/aadd30.

585   Jessen, Søren, Hanne D. Holmslykke, Kristine Rasmussen, Niels Richardt, and Peter E. Holm. 2014. "Hydrology and

586   Pore Water Chemistry in a Permafrost Wetland, Ilulissat, Greenland." Water Resources Research 50 (6): 4760–74.

587   https://doi.org/10.1002/2013WR014376.

588   Kinniburgh, D., and Cooper, D. 2011: PhreePlot: Creating Graphical Output with Phreeqc.

589   Koch, J. C., Runkel, R. L., Striegl, R., and McKnight, D. M. 2013: Hydrologic controls on the transport and cycling

590   of carbon and nitrogen in a boreal catchment underlain by continuous permafrost. Journal of Geophysical Research:

591   Biogeosciences, 118: 698–712, doi: https://doi.org/10.1002/jgrg.20058.

592   Kokelj, S. V., and Jorgenson, M. T. 2013: Advances in Thermokarst Research. Permafrost and Periglacial Processes,

593   24: 108–119, doi: https://doi.org/10.1002/ppp.1779.

594   Kurylyk and Walvoord, 2021 Kurylyk, B.L. and Walvoord, M.A., 2021. Permafrost Hydrogeology. In Arctic

595   Hydrology, Permafrost and Ecosystems (pp. 493-523). Springer, Cham.

596   Langford, Z. L., Kumar, J., Hoffman, F. M., Breen, A. L., & Iversen, C. M. (2019). Arctic vegetation mapping using

597   unsupervised training datasets and convolutional neural networks. Remote Sensing, 11(1), 1–23.

598   https://doi.org/10.3390/rs11010069

599   Lara, M. J., Nitze, I., Grosse, G., and McGuire, A. D. 2018: Tundra landform and vegetation productivity trend maps

600   for the Arctic Coastal Plain of northern Alaska. Scientific Data, 5: 1–10, doi: https://doi.org/10.1038/sdata.2018.58.

601   Léger, E., Dafflon, B., Robert, Y., Ulrich, C., Peterson, J. E., Biraud, S. C., … Hubbard, S. S. 2019: A distributed

602   temperature profiling method for assessing spatial variability in ground temperatures in a discontinuous permafrost

603   region of Alaska. The Cryosphere, 13: 2853–2867, doi: https://doi.org/10.5194/tc-13-2853-2019.

604   Liljedahl, A. K., Boike, J., Daanen, R. P., Fedorov, A. N., Frost, G. V., Grosse, G., … Zona, D. 2016: Pan-Arctic ice-

605   wedge degradation in warming permafrost and its influence on tundra hydrology. Nature Geoscience, 9: 312–318,

606   doi: https://doi.org/10.1038/ngeo2674.

607   McCaully, R. E., Arendt, C. A., Newman, B. D., Salmon, V. G., Heikoop, J. M., Wilson, C. J., Sevanto, S., Wales, N.
608   A., Perkins, G. B., Marina, O. C., and Wullschleger, S. D.: High nitrate variability on an Alaskan permafrost hillslope
609   dominated by alder shrubs, The Cryosphere, 16, 1889–1901, https://doi.org/10.5194/tc-16-1889-2022, 2022.

610   McClelland, J. W., Holmes, R. M., Peterson, B. J., Raymond, P. A., Striegl, R. G., Zhulidov, A. V., … Griffin, C. G.
611   2016: Particulate organic carbon and nitrogen export from major Arctic rivers. Global Biogeochemical Cycles, 30:
612   629–643, doi: https://doi.org/10.1002/2015GB005351.

613   Mitchell, J. S., and Ruess, R. W. (2009). N2 fixing alder (Alnus viridis spp. fruticosa) effects on soil properties across
614   a secondary successional chronosequence in interior Alaska. Biogeochemistry 95, 215–229. doi: 10.1007/s10533-009-
615   9332-x

616   Mulligan, J. J. 1965: Examination of the Sinuk Iron Deposits Seward Peninsula, Alaska. United States Department of
617   the Interior, 37.

618   Myers-Smith, I. H., Forbes, B. C., Wilmking, M., Hallinger, M., Lantz, T., Blok, D., … Hik, D. S. 2011: Shrub
619   expansion in tundra ecosystems: dynamics, impacts and research priorities. Environmental Research Letters, 6:
620   045509, doi: https://doi.org/10.1088/1748-9326/6/4/045509.

621   Nossov, D. R., Hollingsworth, T. N., Ruess, R. W., and Kielland, K. (2011). Development of Alnus tenuifolia stands
622   on an Alaskan floodplain: patterns of recruitment, disease and succession. J. Ecol. 99, 621–633. doi: 10.1111/j.1365-
623   2745.2010.01792.x

624   O'Donnell, J., Douglas, T., Barker, A. and Guo, L., 2021. Changing Biogeochemical Cycles of Organic Carbon,
625   Nitrogen, Phosphorus, and Trace Elements in Arctic Rivers. In Arctic Hydrology, Permafrost and Ecosystems (pp.
626   315-348). Springer, Cham.

627   Patzner, M.S., Kainz, N., Lundin, E., Barczok, M., Smith, C., Herndon, E., Kinsman-Costello, L., Fischer, S., Straub,
628   D., Kleindienst, S., Kappler, A., Bryce, C., 2022. Seasonal Fluctuations in Iron Cycling in Thawing Permafrost
629   Peatlands. Environ. Sci. Technol. 56, 4620–4631. https://doi.org/10.1021/acs.est.1c06937

630   Parkhurst, D., and Appelo, C. A. J. 2013: Description of input and examples for PHREEQC version 3: a computer
631   program for speciation, batch-reaction, one-dimensional transport, and inverse geochemical calculations (USGS
632   Numbered Series No. 6-A43). Reston, VA: U.S. Geological Survey.

633   Perdrial, J. N., Perdrial, N., Vazquez-Ortega, A., Porter, C., Leedy, J., and Chorover, J. 2014: Experimental
634   Assessment of Passive Capillary Wick Sampler Suitability for Inorganic Soil Solution Constituents. Soil Science
635   Society of America Journal, 78: 486–495, doi: https://doi.org/10.2136/sssaj2013.07.0279.

636   Petrone, K. C., Hinzman, L. D., Shibata, H., Jones, J. B., and Boone, R. D. 2007: The influence of fire and permafrost
637   on sub-arctic stream chemistry during storms. Hydrological Processes, 21: 423–434, doi:
638   https://doi.org/10.1002/hyp.6247.

639   Philben, M., Taş, N., Chen, H., Wullschleger, S. D., Kholodov, A., Graham, D. E., and Gu, B. 2020: Influences of
640   hillslope biogeochemistry on anaerobic soil organic matter decomposition in a tundra watershed. Journal of
641   Geophysical Research: Biogeosciences, n/a: e2019JG005512, doi: https://doi.org/10.1029/2019JG005512.

642 Philben, M., Zheng, J., Bill, M., Heikoop, J. M., Perkins, G., Yang, Z., … Gu, B. 2019: Stimulation of anaerobic

643 organic matter decomposition by subsurface organic N addition in tundra soils. Soil Biology and Biochemistry, 130:

644 195–204, doi: https://doi.org/10.1016/j.soilbio.2018.12.009.

645 Prowse, T., Bring, A., Mård, J., and Carmack, E. 2015: Arctic Freshwater Synthesis: Introduction. Journal of

646 Geophysical Research: Biogeosciences, 120: 2121–2131, doi: https://doi.org/10.1002/2015JG003127.

647 Prowse, T., Bring, A., Mård, J., Carmack, E., Holland, M., Instanes, A., … Wrona, F. J. 2015: Arctic Freshwater

648 Synthesis: Summary of key emerging issues. Journal of Geophysical Research: Biogeosciences, 120: 1887–1893, doi:

649 https://doi.org/10.1002/2015JG003128.

650 R Core Team. 2020: R: A Language and Environment for Statistical Computing. Vienna, Austria:, R Foundation for

651 Statistical Computing. Retrieved from https://www.R-project.org/.

652 Raudina, Tatiana V., Sergey V. Loiko, Artyom G. Lim, Ivan V. Krickov, Liudmila S. Shirokova, Georgy I. Istigechev,

653 Daria M. Kuzmina, Sergey P. Kulizhsky, Sergey N. Vorobyev, and Oleg S. Pokrovsky. 2017. "Dissolved Organic

654 Carbon and Major and Trace Elements in Peat Porewater of Sporadic, Discontinuous, and Continuous Permafrost

655 Zones of Western Siberia." Biogeosciences 14 (14): 3561–84. https://doi.org/10.5194/bg-14-3561-2017.

656 Raynolds, M.K.; Walker, D.A.; Maier, H.A. Plant community-level mapping of arctic Alaska based on the

657 Circumpolar Arctic Vegetation Map. Phytocoenologia 2005, 35, 821–848.

658 Raynolds, M. K., Walker, D. A., Balser, A., Bay, C., Campbell, M., Cherosov, M. M., et al. (2019). A raster version

659 of the Circumpolar Arctic Vegetation Map (CAVM). Remote Sensing of Environment, 232.

660 https://doi.org/10.1016/j.rse.2019.111297

661 Romanovsky, V., Cable, W., and Dolgikh, K. 2020a:. Soil Temperature and Moisture, Kougarok Road Mile Marker

662 64, Seward Peninsula, Alaska, beginning 2016 [Data set], doi: https://doi.org/10.5440/1581586.

663 Romanovsky, V., Cable, W., and Dolgikh, K. 2020b:. Soil Temperature and Moisture, Kougarok Road Mile Marker

664 64, Seward Peninsula, Alaska, beginning 2016 [Data set], doi: https://doi.org/10.5440/1581586.

665 Romanovsky, V., Cable, W., and Dolgikh, K. 2020c:. Soil Temperature and Moisture, Teller Road Mile Marker 27,

666 Seward Peninsula, Alaska, beginning 2016 [Data set], doi: https://doi.org/10.5440/1581437.

667 Romanovsky, V., Cable, W., and Dolgikh, K. 2020d:. Soil Temperature and Moisture, Teller Road Mile Marker 27,

668 Seward Peninsula, Alaska, beginning 2016 [Data set], doi: https://doi.org/10.5440/1581437.

669 Rowland, J. C., Jones, C. E., Altmann, G., Bryan, R., Crosby, B. T., Hinzman, L. D., … Geernaert, G. L. 2010: Arctic

670 Landscapes in Transition: Responses to Thawing Permafrost. Eos, Transactions American Geophysical Union, 91:

671 229–230, doi: https://doi.org/10.1029/2010EO260001.

672 Ruess, R. W., Anderson, M. D., Mcfarland, J. M., Kielland, K., Olson, K., and Taylor, D. L. (2013). Ecosystem-level

673 consequences of symbiont partnerships in an N-fixing shrub from interior Alaskan floodplains. Ecol. Monogr. 83,

674 177– 194. doi: 10.1890/12-0782.1

675 Salmon, V. G., Breen, A. L., Kumar, J., Lara, M. J., Thornton, P. E., Wullschleger, S. D., and Iversen, C. M. 2019:

676 Alder Distribution and Expansion Across a Tundra Hillslope: Implications for Local N Cycling. Frontiers in Plant

677 Science, 10, doi: https://doi.org/10.3389/fpls.2019.01099.

678   Schuur, E. A. G., McGuire, A. D., Schädel, C., Grosse, G., Harden, J. W., Hayes, D. J., … Vonk, J. E. 2015: Climate
679   change and the permafrost carbon feedback. Nature, 520: 171–179, doi: https://doi.org/10.1038/nature14338.

680   Shaver, G. R., Billings, W. D., Chapin, F. S., Giblin, A. E., Nadelhoffer, K. J., Oechel, W. C., and Rastetter, E. B.
681   1992: Global Change and the Carbon Balance of Arctic Ecosystems. BioScience, 42: 433–441, doi:
682   https://doi.org/10.2307/1311862.

683   Shogren, A. J., Zarnetske, J. P., Abbott, B. W., Iannucci, F., Frei, R. J., Griffin, N. A., and Bowden, W. B. 2019:
684   Revealing biogeochemical signatures of Arctic landscapes with river chemistry. Scientific Reports, 9: 1–11, doi:
685   https://doi.org/10.1038/s41598-019-49296-6.

686   Smith, L. C., Sheng, Y., MacDonald, G. M., and Hinzman, L. D. 2005: Disappearing Arctic Lakes. Science, 308:
687   1429–1429, doi: https://doi.org/10.1126/science.1108142.

688   Sparks, D. L. 2003: Environmental soil chemistry (2nd ed). Amsterdam ; Boston:, Academic Press, 352 pp.

689   Spence, C., Kokelj, S., McCluskie, M., and Hedstrom, N. 2015: Impacts of Hydrological and Biogeochemical Process
690   Synchrony Transcend Scale. In AGU Fall Meeting Abstracts (Vol. 2015).

691   Sturm, M., Racine, C., and Tape, K. 2001: Increasing shrub abundance in the Arctic. Nature, 411: 546–547, doi:
692   https://doi.org/10.1038/35079180.

693   Sulman, B. N., Salmon, V. G., Iversen, C. M., Breen, A. L., Yuan, F., & Thornton, P. E. (2021). Integrating arctic
694   plant functional types in a land surface model using above- and belowground field observations. Journal of Advances
695   in Modeling Earth Systems, 13, e2020MS002396. https://doi. org/10.1029/2020MS002396

696   Tape, K. D., Hallinger, M., Welker, J. M., and Ruess, R. W. 2012: Landscape Heterogeneity of Shrub Expansion in
697   Arctic Alaska. Ecosystems, 15: 711–724, doi: https://doi.org/10.1007/s10021-012-9540-4.

698   Tape, K., Sturm, M., and Racine, C. 2006: The evidence for shrub expansion in Northern Alaska and the Pan-Arctic.
699   Global Change Biology, 12: 686–702, doi: https://doi.org/10.1111/j.1365-2486.2006.01128.x.

700   Till, A. B., Dumoulin, J. A., Werdon, M. B., and Bleick, H. A. 2011: Bedrock geologic map of the Seward Peninsula,
701   Alaska, and accompanying conodont data. US Department of the Interior, US Geological Survey.

702   Uren, N. C. 2018: Calcium oxalate in soils, its origins and fate – a review. Soil Research, 56: 443, doi:
703   https://doi.org/10.1071/SR17244.

704   Vonk, J. E., Tank, S. E., Bowden, W. B., Laurion, I., Vincent, W. F., Alekseychik, P., … Wickland, K. P. 2015:
705   Reviews and syntheses: Effects of permafrost thaw on Arctic aquatic ecosystems. Biogeosciences, 12: 7129–7167,
706   doi: https://doi.org/10.5194/bg-12-7129-2015.

707   Vonk, J. E., Tank, S. E., and Walvoord, M. A. 2019: Integrating hydrology and biogeochemistry across frozen
708   landscapes. Nature Communications, 10: 1–4, doi: https://doi.org/10.1038/s41467-019-13361-5.

709   Walker, D. A., Breen, A. L., Druckenmiller, L. A., Wirth, L. W., Fisher, W., Raynolds, M. K., Sibik, J., Walker, M.
710   D., Hennekens, S., Boggs, K., Boucher, T., Buchhorn, M., Bultmann, H., Cooper, D. J., Daniels, F. J. A., Davidson,
711   S. J., Ebersole, J. J., Elmendorf, S. C., Epstein, H. E., Gould, W. A., Hollister, R. D., Iversen, C. M., Jorgenson, M.
712   T., Kade, A., Lee, M. T., MacKenzie, W. H., Peet, R. K., Peirce, J. L., Schickhoff, U., Sloan, V. L., Talbot, S. S.,
713   Tweedie, C. E., Villarreal, S., Webber, P. J., and Zona, D.: The Alaska Arctic Vegetation Archive (AVA-AK),
714   Phytocoenologia, 46, 221–229, https://doi.org/10.1127/phyto/2016/0128, 2016.

715   Wallenberger, F. T., and Bingham, P. A. 2009: Fiberglass and Glass Technology: Energy-Friendly Compositions and

716   Applications. Springer Science & Business Media, 479 pp.

717   Walvoord, M. A., and Kurylyk, B. L. 2016: Hydrologic Impacts of Thawing Permafrost—A Review. Vadose Zone

718   Journal, 15, doi: https://doi.org/10.2136/vzj2016.01.0010.

719   Weiss, M., Hobbie, S. E., & Gettel, G. M. (2005). Contrasting Responses of Nitrogen-Fixation in Arctic Lichens to

720   Experimental and Ambient Nitrogen and Phosphorus Availability. Arctic, Antarctic, and Alpine Research, 37(3), 396–

721   401. https://doi.org/10.1657/1523-0430(2005)037[0396:CRONIA]2.0.CO;2

722   Wilson, C., Bolton, R., Busey, R., Lathrop, E., and Dann, J. 2019: End-of-Winter Snow Depth, Temperature, Density

723   and SWE Measurements at Kougarok Road Site, Seward Peninsula, Alaska, 2018 [Data set], doi:

724   https://doi.org/10.5440/1593874.

725   Wilson, C., Bolton, R., Busey, R., Lathrop, E., Dann, J., and Charsley-Groffman, L. 2019: End-of-Winter Snow Depth,

726   Temperature, Density and SWE Measurements at Teller Road Site, Seward Peninsula, Alaska, 2016-2018 [Data set],

727   doi: https://doi.org/10.5440/1592103.

728   Wilson, C., Dann, J., Bolton, R., Charsley-Groffman, L., Jafarov, E., Musa, D., and Wullschleger, S. 2021: In Situ

729   Soil Moisture and Thaw Depth Measurements Coincident with Airborne SAR Data Collections, Barrow and Seward

730   Peninsulas, Alaska, 2017 [Data set], doi: https://doi.org/10.5440/1423892.

731   Wrona, F. J., Johansson, M., Culp, J. M., Jenkins, A., Mård, J., Myers-Smith, I. H., … Wookey, P. A. 2016: Transitions

732   in Arctic ecosystems: Ecological implications of a changing hydrological regime. Journal of Geophysical Research:

733   Biogeosciences, 121: 650–674, doi: https://doi.org/10.1002/2015JG003133.

734   Wullschleger, S. D., Epstein, H. E., Box, E. O., Euskirchen, E. S., Goswami, S., Iversen, C. M., et al. (2014). Plant

735   functional types in earth system models: past experiences and future directions for application of dynamic vegetation

736   models in high-latitude ecosystems. Ann. Bot. 114, 1–16. doi: 10.1093/aob/mcu077

737   Yang, D., Meng, R., Morrison, B. D., McMahon, A., Hantson, W., Hayes, D. J., … Serbin, S. P. 2020: A Multi-Sensor

738   Unoccupied Aerial System Improves Characterization of Vegetation Composition and Canopy Properties in the Arctic

739   Tundra. Remote Sensing, 12: 2638, doi: https://doi.org/10.3390/rs12162638.

740   Yang, D., et al. "Landscape-Scale Characterization of Arctic Tundra Vegetation Composition, Structure, and Function

741   with a Multi-Sensor Unoccupied Aerial System." Environmental Research Letters 16 (8), 085005 (2021).

742   https://doi.org/10.1088/1748-9326/ac1291.

743

744   **8. Figures**
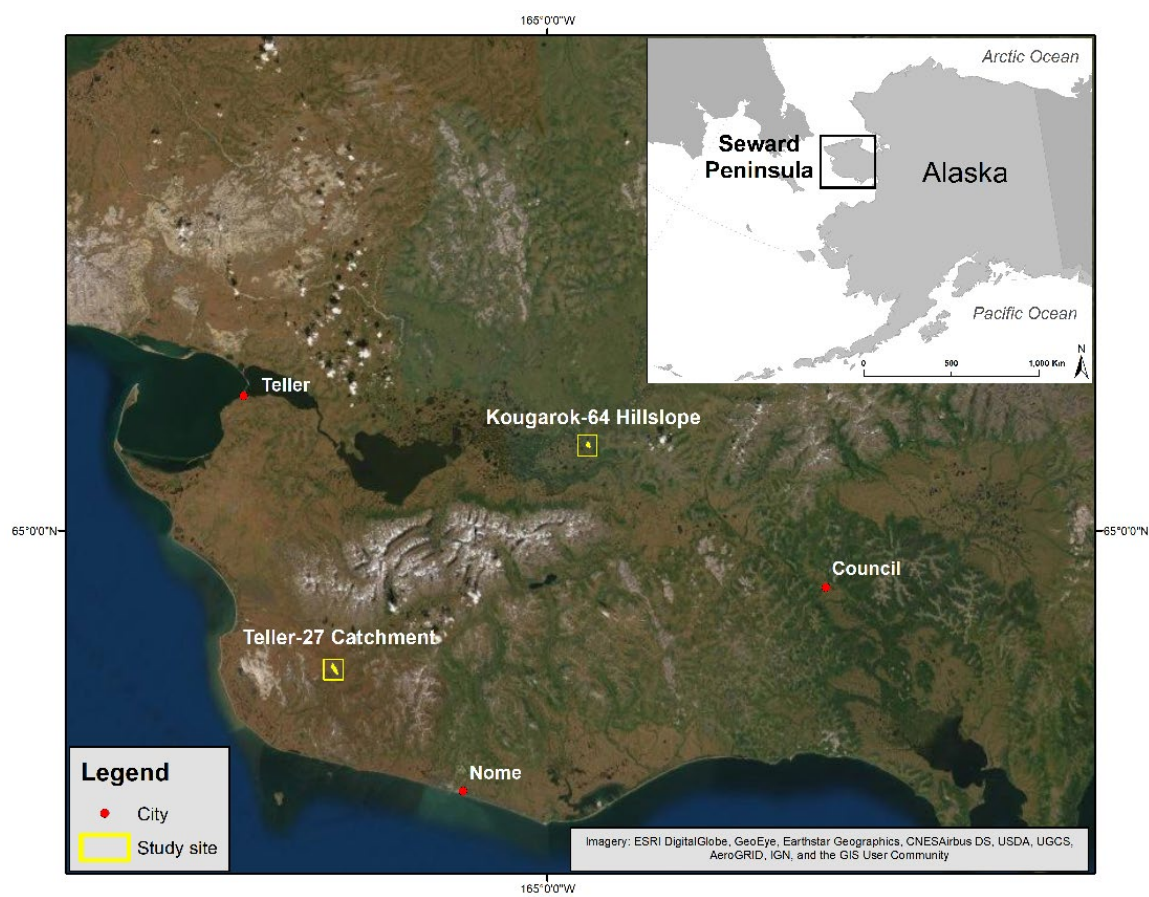
745

746   **Figure 1. Location of the Teller and Kougarok field sites with respect to the municipalities of Teller, Nome, and Council.**
747   **All are located on the Seward Peninsula in northwestern Alaska. RGB composite imagery from the 8-band WorldView-2**
748   **imagery obtained on July 14, 2017 at 1.5 m resolution downloaded from the DigitalGlobe website**
749   **(https://www.digitalglobe.com/).**

750
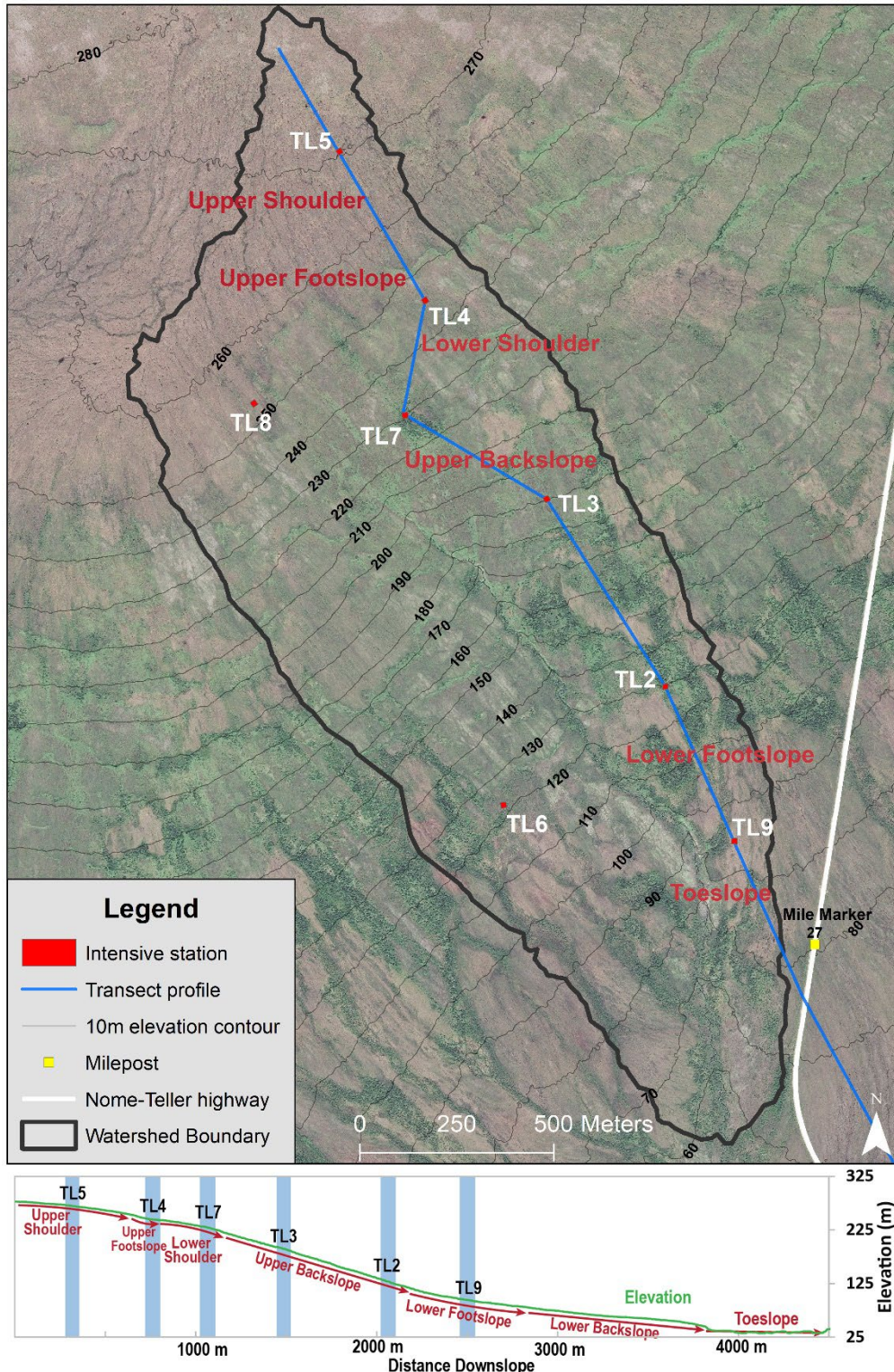
751

752 **Figure 2. Topographic map of Teller. Station areas are shown as red polygons and the topographic station transect is given**
753 **as a solid blue line. The hillslope transect elevation profile is given below the map in green, with stations along the transect**
754 **in blue and hillslope positions noted with red arrows and text. RGB composite imagery from the 8-band WorldView-2**
755 **imagery obtained on July 27, 2011 at 1.5 m resolution downloaded from the DigitalGlobe website**
756 **(https://www.digitalglobe.com/).**

757

758
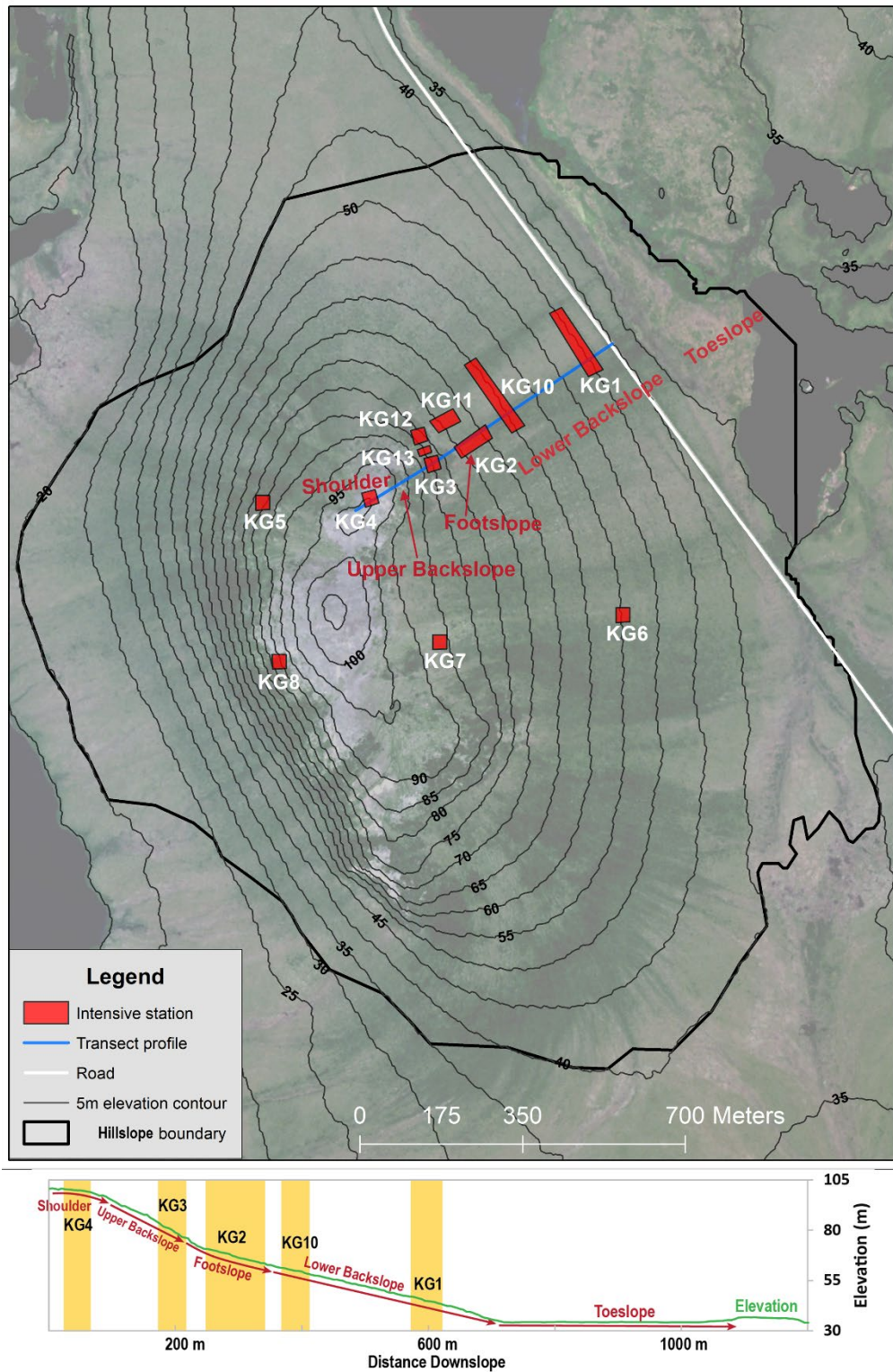
Figure 3. Topographic map of Kougarok. Station areas are shown as red polygons and the station transect is given as a solid blue line. The transect elevation profile is given below the map in green, with stations along the transect in yellow and hillslope positions noted with red arrows and text. RGB composite imagery from the 8-band WorldView-2 imagery obtained on July 14, 2017 at 1.5 m resolution downloaded from the DigitalGlobe website (https://www.digitalglobe.com/).

763

764
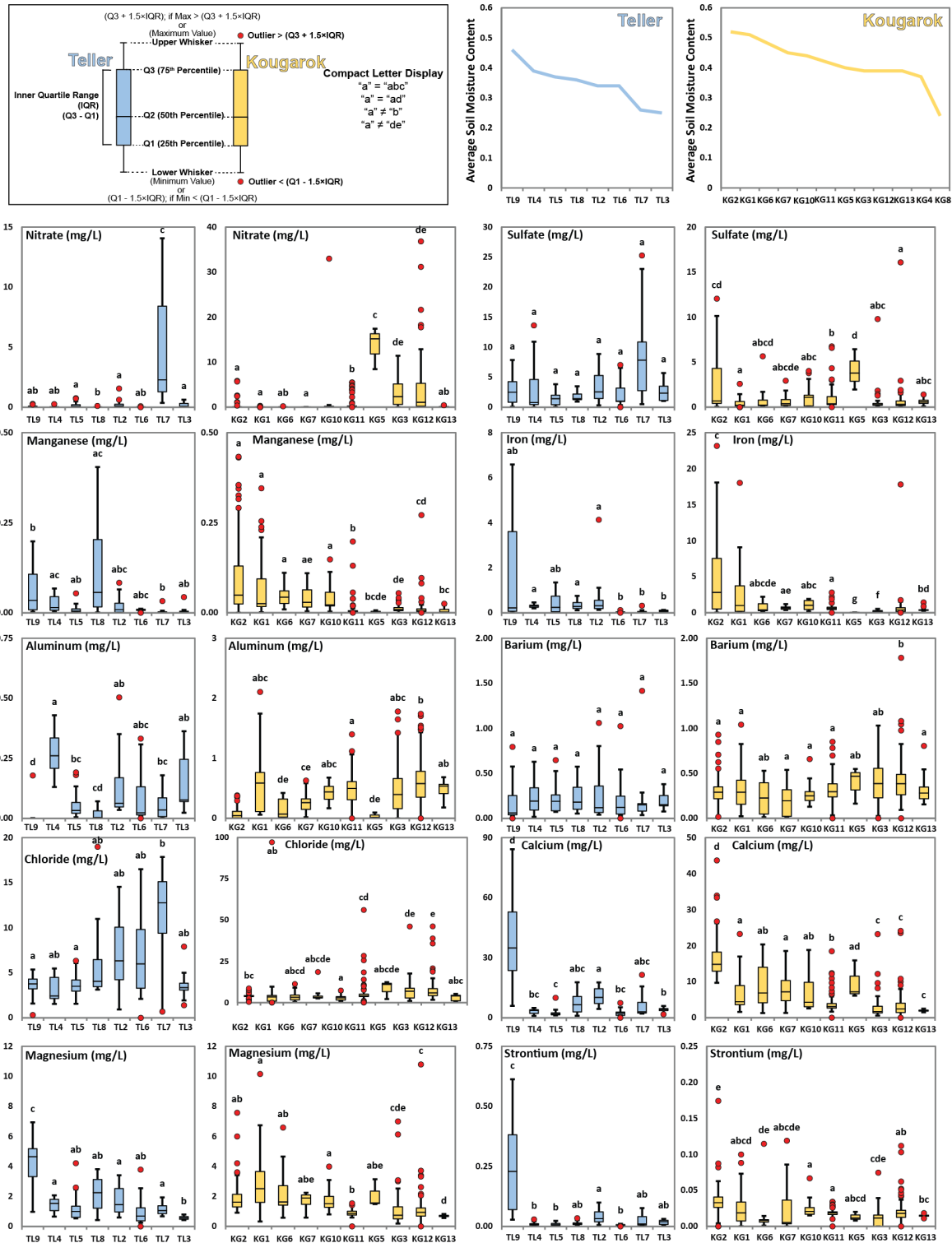
765 **Figure 4. Mean COI concentrations at Teller (blue) and Kougarok (yellow) stations. Stations are arranged (left to right) by**
766 **soil moisture content determined by P-Band SAR (top right). Boxplots show the first, second, and third data quartiles, with**
767 **box whiskers representing either 150% of the inner quartile range (IQR), or the maximum or minimum value, when that**
768 **value was less than 1.5×IQR. Red circles represent data points outside of the 1.5×IQR whiskers (i.e. outliers). Note that the**
769 **concentration scales on the Teller and Kougarok plots often differ.**

770

771
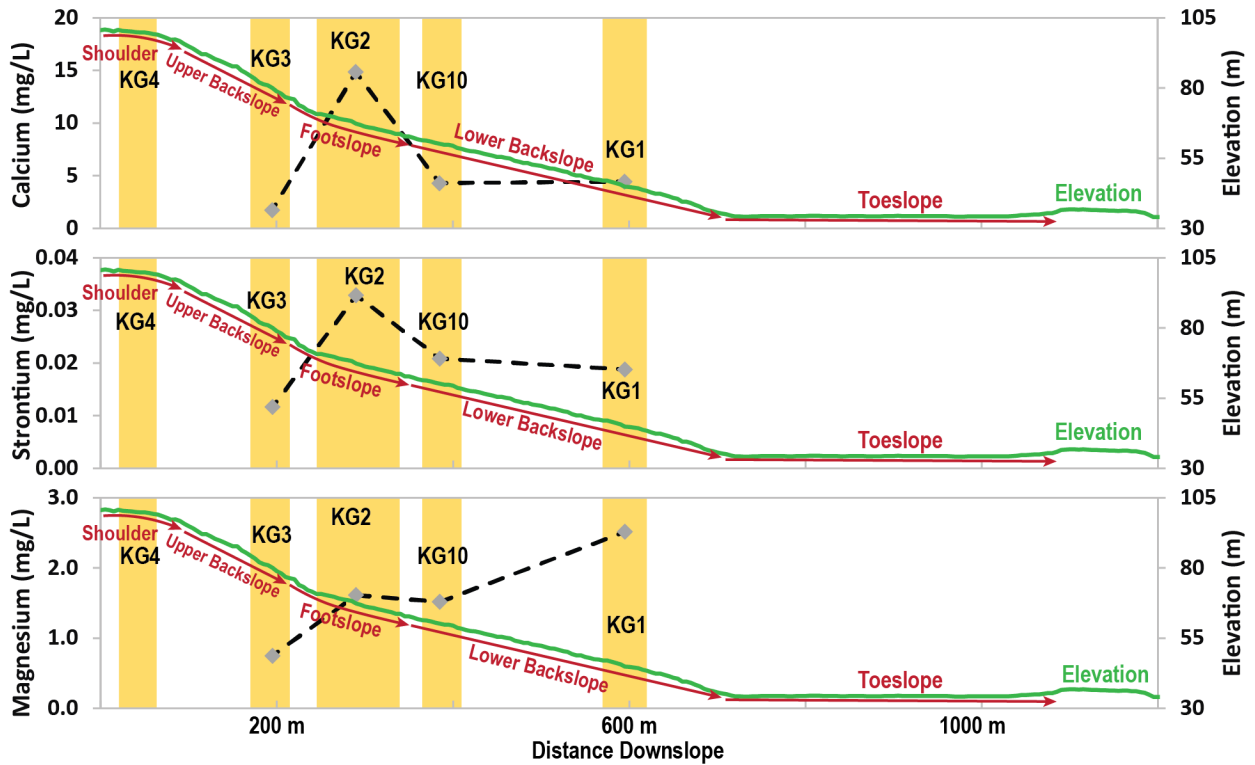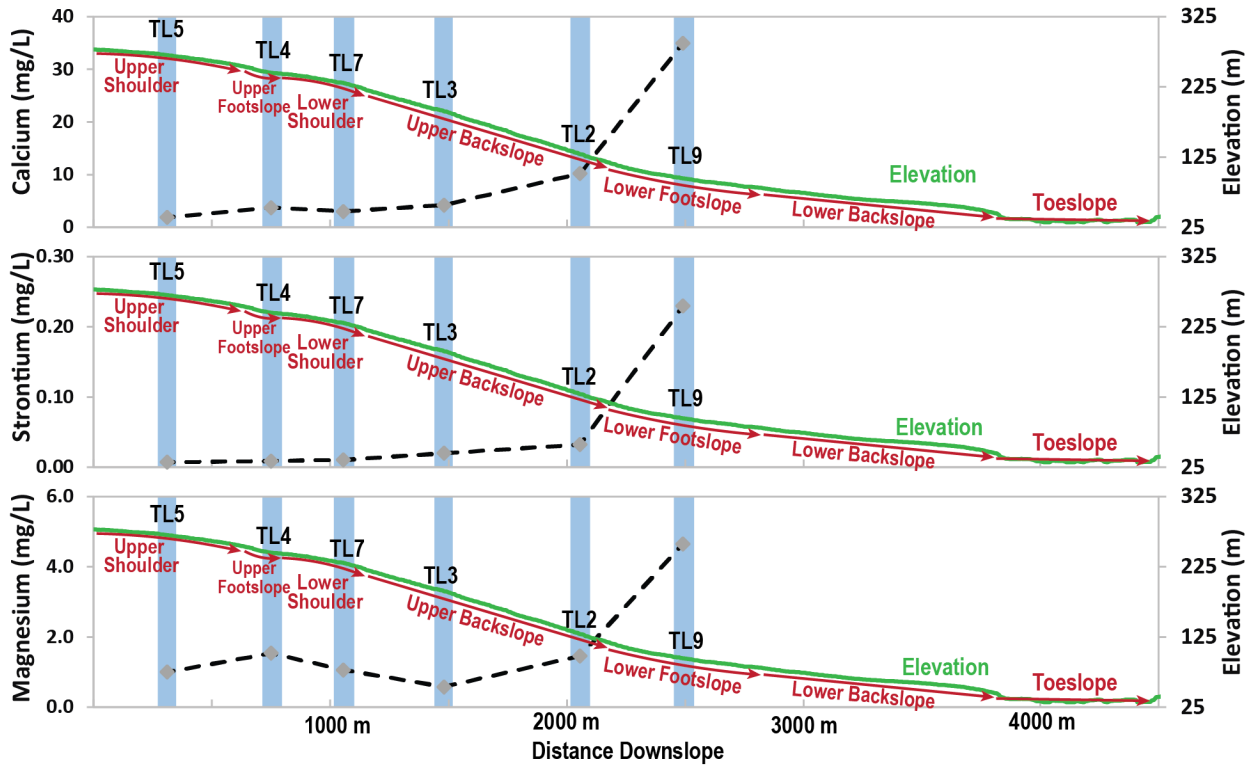
Figure 5. Median (50th percentile) concentrations (grey diamonds with dashed black lines) of Ca, Sr, and Mg, with distance downslope at Teller (blue) and Kougarok (yellow) along topographic transects; areas of stations are indicated by blue and yellow colouring, respectively. The elevation profiles of the hillslopes are plotted in green, on separate y-axes (right axes). Topographic regions of both catchments are indicated by red arrows along the elevation gradient.
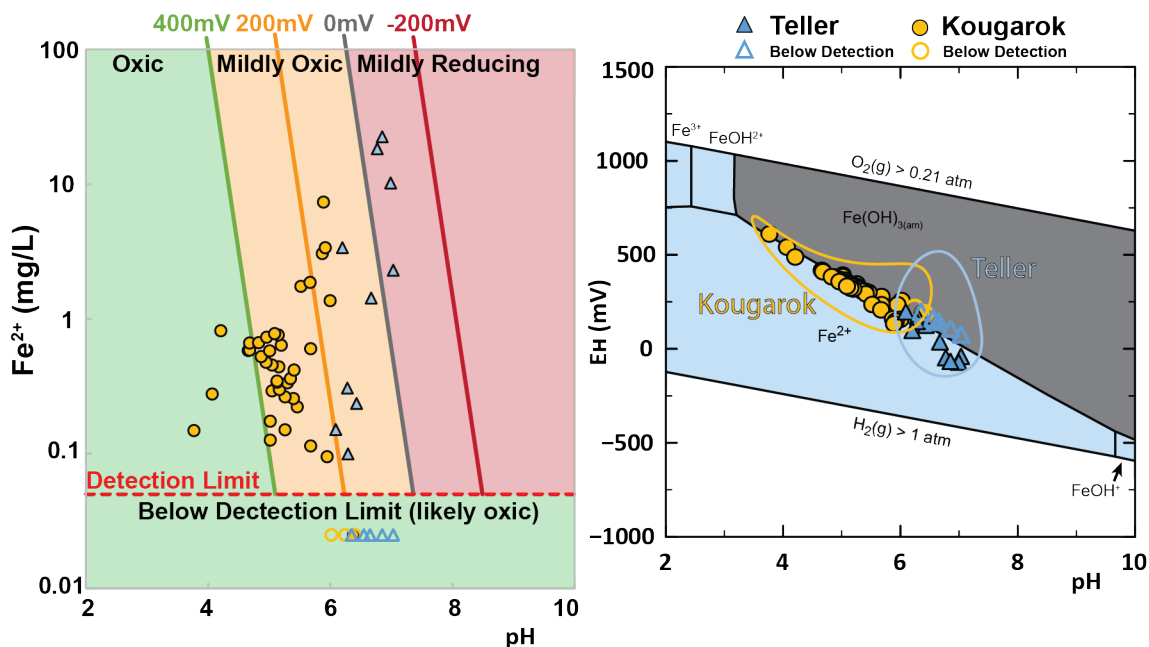
Figure 6. Left: Model-predicted Fe^{2+} concentrations in saturated solutions of $Fe(OH)_{3(am)}$ at fixed E_H conditions of 400 mV (green), 200 mV (orange), 0 mV (grey), and -200 mV (red), compared with field concentrations of Fe^{2+} at Teller (red circles) and Kougarok (yellow circles). **Right:** Fe predominance diagram, showing the dominant specie of Fe under a range of E_H/pH conditions. E_H/pH regions relevant to Teller and Kougarok are outlined in blue and yellow, respectively. Samples with Fe^{2+} concentrations below the detection limit are given as colour coordinated open circles set at 0.025 mg·L^{-1} (half the detection limit) in both sides of the figure.
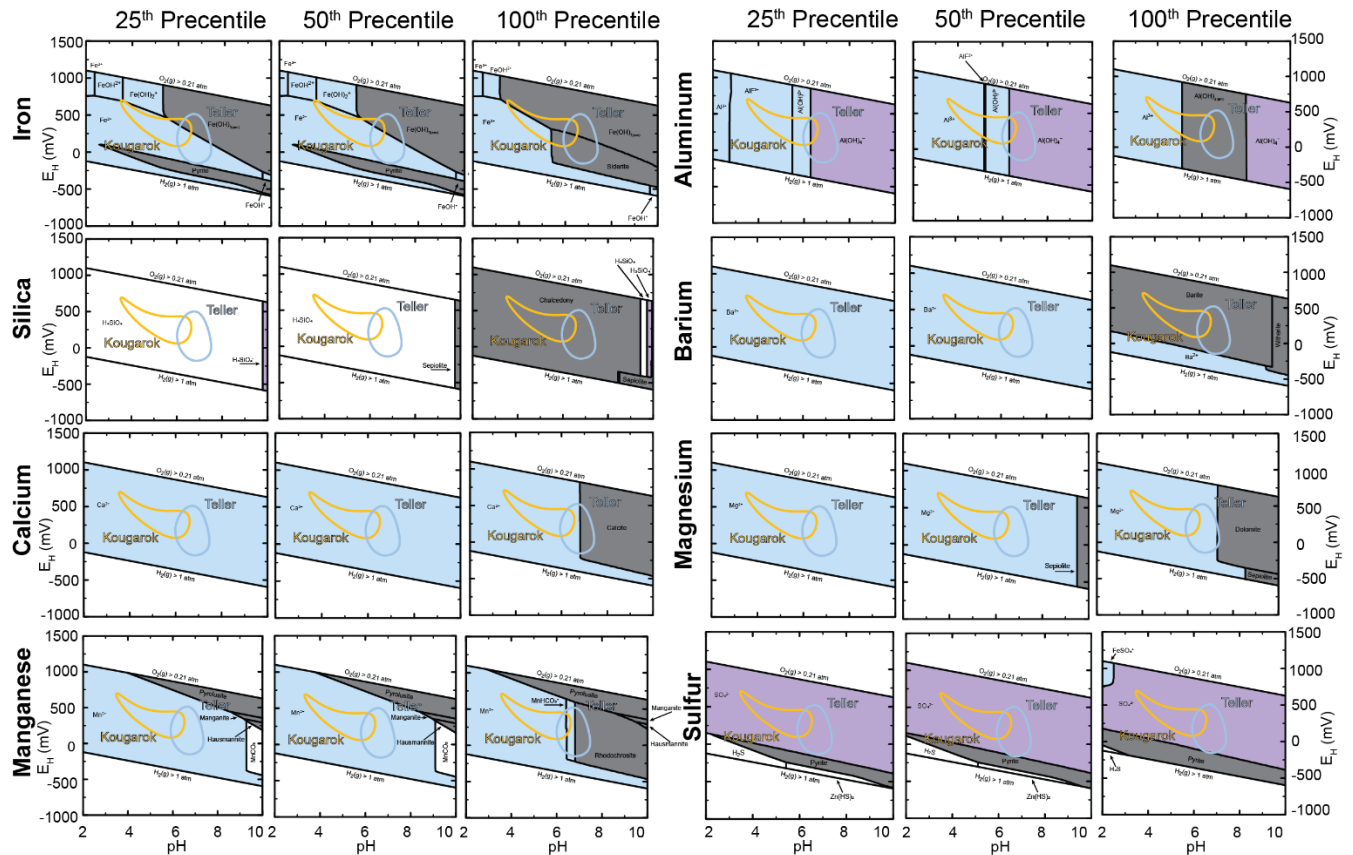
Figure 7. E_H/pH diagrams for key species that indicated possible mineral formation under the E_H/pH conditions present at either Teller or Kougarok. The E_H and pH conditions observed at Teller and Kougarok are overlaid as blue and yellow lines, respectively. Mineral species (solids) are shown in grey, cations on are shown in blue, anions are shown in purple, neutral species are shown in white. Predominance diagrams were created in PhreePlot using the phreeqc.dat database, with inorganic carbonate reduction to methane "turned off."

791

792
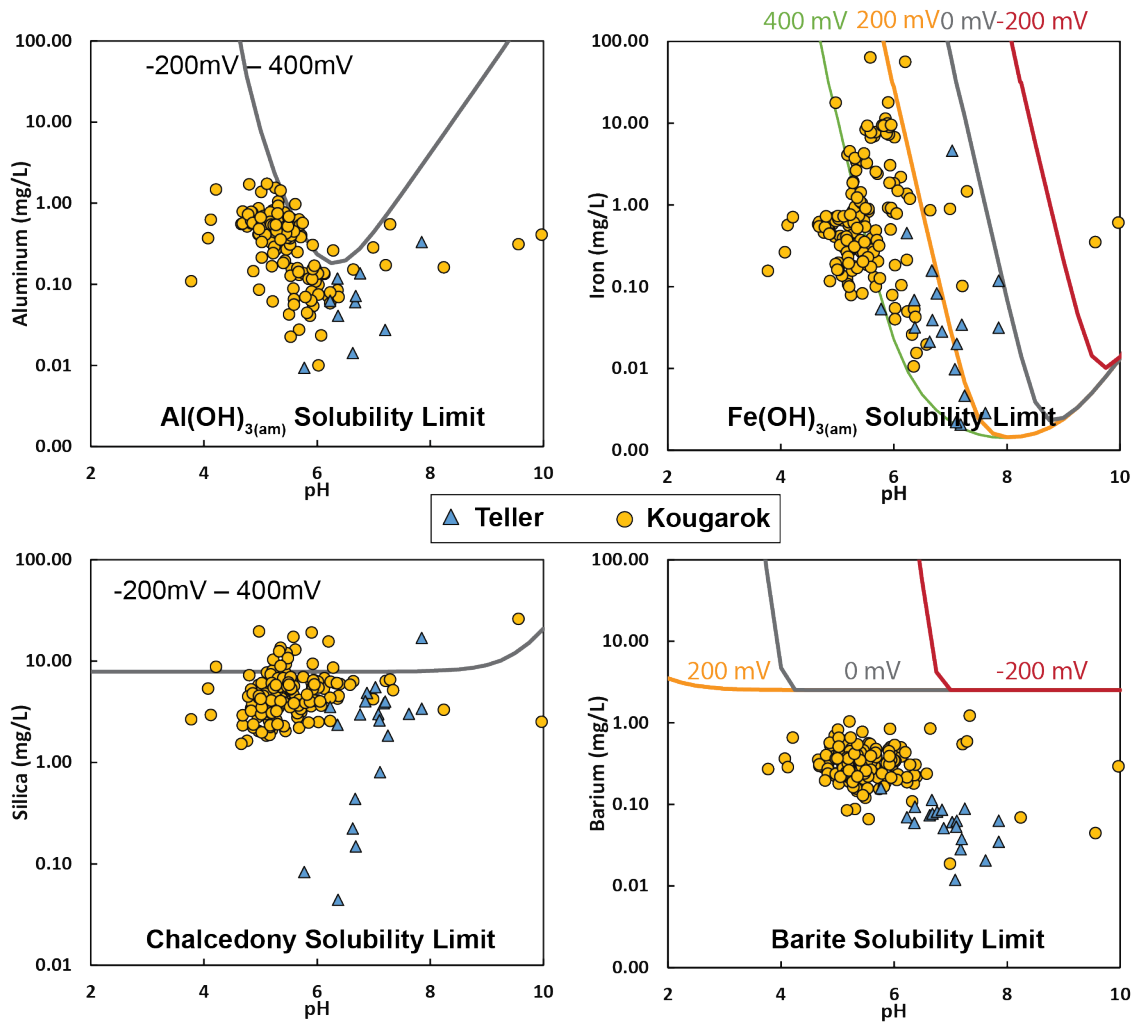
Figure 8. Modelled solute concentrations in solutions saturated with Al(OH)$_{3(am)}$, Fe(OH)$_{3(am)}$, chalcedony, and barite, with respect to pH (x-axis) and E$_H$ (model lines), overlaid with observed solute concentrations.

795

9. Tables

Table 1. Teller Station Physical Characteristics

	Hillslope Position	Vegetation type	Average (maximum) canopy height (cm)	Dominant PFT		Low to tall shrub cover	Average TDR soil moisture (VMC)	Average P-band SAR (VMC)	Average snow depth (cm)	Average Ground Temperature (°C)	Permafrost Extent	Average (maximum) thaw depth (cm)
				Vegetation				*Relative wetness*		*Permafrost*		
TL9	Lower Footslope		28 (41)	Bryophyte	44 %	10 %	NA	0.46	68.4	0	Marginal	101 (>120)
TL5	Upper Shoulder	Wetland complex	12 (45)	Graminoid	45 %	7 %	0.55	0.37	103.3	-0.45	Near-surface	97ʳ (>114ʳ)
TL8	Upper Footslope		7 (34)	Bryophyte	33 %	20 %	0.55	0.36	77.7	-0.6		69ʳ (>120)
TL3	Upper Backslope	Cassiope dwarf shrub tundra	9 (23)	Evergreen dwarf shrub	47 %	12 %	NA	0.25	62.1	2.2	None/ deep	72ʳ (82ʳ)
TL4	Upper Footslope		8 (14)		58 %	4 %	0.35	0.39	89.5	0.5	Marginal	40ʳ (70ʳ)
TL2	Upper Backslope	Mesic willow shrubland	84 (141)	Deciduous low to tall shrub (willow)	44 %	44 %	0.4	0.34	124	2.4	None/ deep	75ʳ (>120)
TL7	Lower Shoulder		151 (189)		37 %	37 %	0.46	0.26	128.8	2.4		51ʳ (66ʳ)
TL6	Upper Backslope	Willow-birch tundra	64 (115)	Forb	23 %	32 %	0.38	0.34	86.4	1.2	None/ deep	67rʳ (102ʳ)

798

PFT – plant functional type; dwarf shrub (height <40 cm), low shrub (height 40-200 cm), low to tall shrub (height 40 to >200 cm tall). Deciduous shrub PFT classes identify the dominant species in the plant community as either willow or willow and birch. There is no alder at the Teller site. Low to tall shrub cover represents the sum of deciduous low shrubs, deciduous low to potentially tall willow and birch, and deciduous low to tall alder.

[1]Single point soil moisture measurements. Data are more accurate than P-band SAR but represent a much smaller spatial scale.

[2]P-band SAR has 30m resolution.

ʳResistive layer was rock; all others are permafrost. A temperature probe was used to determine if the resistive layer was permafrost (≤0 °C) or rock (>2 °C). Thaw depth is an average of 4 measurements from the vegetation plot corners within the IS and was measured at the end of the growing season.

808

Table 2. Kougarok Station Physical Characteristics

		Vegetation					Relative wetness			Permafrost		
	Hillslope Position	Vegetation type	Average (maximum) canopy height (cm)	Dominant PFT		Low to tall shrub cover	Average TDR soil moisture (VMC)	Average P-band SAR (VMC)	Average snow depth (cm)	Average Ground Temperature (°C)	Permafrost Extent	Average (maximum) thaw depth (cm)
KG3	Upper Backslope	Alder shrubland	204 (265)	Deciduous low to tall shrub (alder)	30 %	53 %	0.19	0.39	131.3	-0.01	Near-surface	48[r] (53[r])
KG12	Footslope		NA	NA	NA	NA	0.30*	0.39	NA	NA		NA
KG1	Lower Backslope	Alder savanna in tussock tundra	60 (90)	Deciduous low shrub	31 %	44 %	NA	0.51	83.4	-2.5		61 (68)
KG2	Footslope		48 (73)	Graminoid	30 %	42 %	0.63	0.52	102.3	-1.2	Near-surface	75 (89)
KG6	Lower Backslope		24 (61)	Graminoid	46 %	17 %	0.36	0.48	66.2	-2.2		58 (62)
KG10	Lower Backslope		NA	NA	NA	NA	NA*	0.44	71.4	NA		NA
KG11	Footslope		NA	NA	NA	NA	0.59*	0.42	NA	NA		NA
KG7	Upper Backslope	Tussock-lichen tundra	20 (22)	Graminoid	34 %	14 %	0.51	0.45	54.7	-2.1	Near-surface	76 (100)
KG4	Shoulder	Dryas-lichen shrub tundra	6 (12)	Evergreen dwarf shrub	62 %	1 %	NA	0.37	NA	-1.9	Near-surface	0[r] (0[r])
KG13	Upper Backslope		NA	NA	NA	NA	0.41*	0.39	92.1	NA		NA
KG5	Upper Backslope	Willow-birch tundra	62 (137)	Deciduous low shrub	60 %	62 %	NA	0.4	178.4	> 0	Deep	88 (96)
KG8	Upper Backslope		45 (120)	Evergreen dwarf shrub	52 %	42 %	0.23	0.24	85.5	-0.04	Near-surface	44[r] (55[r])

Note: PFT – plant functional type. Deciduous shrub PFT classes identify the dominant species in the community as either willow, alder, willow and birch, or alder, willow, and birch. Low to tall shrub cover represents the sum of deciduous low shrubs, deciduous low to potentially tall willow and birch, and deciduous low to tall alder.
[1]Single point soil moisture measurements. Data are more accurate than P-band SAR but represent a much smaller spatial scale.
[2]P-band SAR has 30m resolution.
*Average gravimetric water content measurements, corrected to VMC by bulk density.
[r]Resistive layer was rock; all others are permafrost. A temperature probe was used to determine if the resistive layer was permafrost (≤ 0 °C) or rock (>2 °C). Thaw depth is an average of 4 measurements from the vegetation plot corners within the IS and was measured at the end of the growing season.

Table 3. Inter-Site Mann-Whitney U-Test Results

	Teller			Kougarok			|z|	Site with Higher Median	Effect Size	Difference in Correlation
	n	$\sum R_i$	U_i	n	$\sum R_i$	U_i				
Na	59	3184	14811.5	275	52761.5	1413.5	**9.95**	Kougarok	0.54	large
F	59	3502	14375.5	273	51776.5	1731.5	**9.46**	Kougarok	0.52	large
K	59	3882	14113	275	52063	2112	**8.92**	Kougarok	0.49	medium-large
Si	59	4119	13876.5	275	51826.5	2348.5	**8.56**	Kougarok	0.47	medium-large
Al	58	4952	12709	275	50659	3241	**7.11**	Kougarok	0.39	medium
Oxalate	57	4996	12161.5	272	49289.5	3342.5	**6.75**	Kougarok	0.37	medium
B	59	5429	12566.5	275	50516.5	3658.5	**6.62**	Kougarok	0.36	medium
Zn	58	5605	12056	275	50006	3894	**6.12**	Kougarok	0.34	medium
SO_4	58	13653	3892.5	273	41293.5	11941.5	**6.08**	Teller	0.33	medium
Fe	58	5958	11703	275	49653	4247	**5.60**	Kougarok	0.31	medium
Ba	58	6256	11405.5	275	49355.5	4544.5	**5.15**	Kougarok	0.28	medium
Ti	58	6266	11395.5	275	49345.5	4554.5	**5.13**	Kougarok	0.28	medium
NO_2	54	5588	10585.5	272	47713.5	4102.5	**5.12**	Kougarok	0.28	medium
Li	58	7778	9883	275	47833	6067	**2.86**	Kougarok	0.16	small-medium
Br	58	8485	9060.5	273	46461.5	6773.5	1.73	Equal	0.09	small
NO_3	58	8576	8969	273	46370	6865	1.59	Kougarok	0.09	small
Sr	58	8683	8978	275	46928	6972	1.51	Kougarok	0.08	small
PO4	54	9659	6460.5	271	43316.5	8173.5	1.36	Equal	0.08	small
Mg	58	10495	7166	275	45116	8784	1.21	Teller	0.07	small
Cr	58	8884	8777	275	46727	7173	1.20	Kougarok	0.07	small
Mn	58	9164	8497	275	46447	7453	0.78	Teller	0.04	small
Cl	58	9221	8266.5	272	45394.5	7509.5	0.57	Kougarok	0.03	small
Ca	58	10016	7645	275	45595	8305	0.50	Teller	0.03	small

Table 4. Dominant Environmental Controls on SPW Geochemistry at Teller and Kougarok

Environmental Control	Analytes Affected
Vegetation	NO_3^-
Soil Moisture/Redox	NO_3^-, Mn, Fe, SO_4 (occasionally)
Water/Soil Interactions & Hydrologic Transport	Ca, Mg, Sr
Mineral Solubility	Al, Ba, Si, Fe